UNIVERSITY OF CALIFORNIA,

IRVINE

Stability Analysis for 1st and 2nd Order Soliton Raman Lasers

THESIS

submitted in partial satisfaction of the requirements

for the degree of

MASTER OF SCIENCE

In Electrical and Computer Engineering

by

Salih Kagan Kalyoncu

Thesis Committee:

Prof. Ozdal Boyraz, Chair

Prof. Nader Bagherzadeh

Prof. Filippo Capolino

2010

ProQuest LLC
789 East Eisenhower Parkway
P.O. Box 1346
Ann Arbor, MI 48106-1346

TABLE OF CONTENTS

LIST OF FIGURES

LIST OF TABLES

ACKNOWLEDGEMENTS

I would like to acknowledge my advisor Prof. Ozdal Boyraz for giving me the opportunity to work with him, and for all his valuable advice, guidance and encouragement during my graduate study. I would also like to thank all of my committee members for their accepting to be in my committee.

In addition, special thanks to my parents Ikram Kalyoncu and Raziye Kalyoncu, my sister Sule Kalyoncu, my wife Guldane Durukan Kalyoncu, and my friends Yusuf Ilerisoy, Yusuf Varli, Yusuf Yigit, Can Eren, Onder Altinkurt and Mehmet Ozkan for supporting and encouraging me to pursue this degree. Without their guidance and continuous help this thesis would not have been possible.

ABSTRACT OF THE THESIS

Stability Analysis for 1st and 2nd Order Soliton Raman Lasers

By

Salih Kagan Kalyoncu

Master of Science in Electrical and Computer Engineering

University of California, Irvine, 2010

Professor Ozdal Boyraz, Chair

Wavelength tunable coherent light sources are highly desired for several applications such as sensing, communications and spectroscopy. In particular, phase coherent light sources with spectral separation of 1000cm^{-1} are widely utilized for applications to detect organic molecules through Coherent Anti-stokes Raman Scattering (CARS) microscopy. However, lack of stable sources that can generate multiple wavelengths with up to 1000cm^{-1} frequency separation mitigates the high efficiency detection process.

This thesis is devoted to the investigation of Raman based soliton lasers that can provide optical sources with 1000cm^{-1} wavelength separation and high peak power. In particular, second order soliton Raman lasers are investigated and theoretical analysis performed to illustrate design criteria for such lasers and to discuss stability conditions. The results provide roadmap to development of such lasers pumped at 1550nm and 1060nm by using commercially available optical fibers.

INTRODUCTION

Throughout the years, an intensive research has been conducted in the development of short-pulse fiber-optical sources for such many applications ranging from optical telecommunications to ultrafast spectroscopy. The common method to generate short pulses in the fiber is the use of spectral broadening induced by nonlinear interactions which result in soliton shaping in anomalous dispersion regime. However, to generate ultra-short pulses, it is also required to have a broadband gain mechanism. [1] Stimulated Raman scattering with a wide gain bandwidth of ~6THz enables to generate femtosecond pulses. Raman gain with the advantage of its being obtained in any nonlinear medium at any wavelength by synchronous pumping, can act as a suitable source. In recent years, Raman fiber lasers have retrieved strong interest due to their capability of serving as pump sources in gain-flattened amplifiers for optical communication systems and as widely tunable sources to characterize the optical devices at longer wavelengths. [2-3] The fixed-wavelength Raman lasers have been widely studied in the last years, but recently, much focus has been on the multi wavelength tunable Raman fiber lasers which generate output Stokes pulses in a broad wavelength range by so called cascaded stimulated Raman scattering. [4] The Raman Solitons generated experimentally near 1.5um by pumping at 1.06um have been reported. [5]

This thesis aimed to design and discuss the stability performance of the high peak power tunable coherent light sources with 1000cm^{-1} frequency separation that can find a perfect application in many fields. In particular, the nonlinear interactions, optical soliton formation and Raman effect inside the fiber are studied to obtain a theoretical model for the generation of Raman soliton laser. Design criteria for both first and the second order

Raman Soliton lasers are suggested. Also, by using Split Step Fourier Method as a simulation tool the stability analyses are conducted for parameters from commercially available optical fibers. In conclusion I show that stable soliton pulses can be generated at 1st and the 2nd Stokes wavelengths with sub-picosecond pulse widths varying from 300fs to 1ps.

CHAPTER 1

NONLINEAR INTERACTIONS IN FIBERS AND THEORY OF RAMAN

The optical pulses while propagating inside a fiber are influenced by both dispersive and nonlinear effects. Fiber as a dispersive medium becomes nonlinear especially for the short pulses with widths ranging from ~10ns to 10fs. Both nonlinear and the dispersive effects cause changes in pulse shape and spectra. According to slowly varying envelope approximation in which the spectral width of the pulse is assumed as much smaller than the incident field frequency, the pulse propagation inside an optical fiber is governed by the Nonlinear Schrodinger Equation (NSE). [5]

$$\frac{\partial A}{\partial z} + \beta_1 \frac{\partial A}{\partial t} - i\frac{1}{2}\beta_2 \frac{\partial^2 A}{\partial t^2} + \frac{\alpha}{2} A + i\gamma |A|^2 A = 0 \tag{1.1}$$

The different terms in the equation (1.1) describe the effects of group velocity, group velocity dispersion (GVD), fiber loss, and fiber non-linearity. The $\gamma = \frac{n_2 \omega_0}{c A_{eff}}$ is the nonlinearity coefficient of the propagation medium.

1.1 Group Velocity Dispersion (GVD)

Group velocity is defined as the effective velocity of wave envelope which has different frequency components. An optical medium in which the waves having different frequencies travel at different velocity is called dispersive medium. Dispersion may originate from the nature of the material (material dispersion) used for light propagation

and design of the optical waveguides such as its geometry and materials used in core and cladding part of the waveguide. In an optical fiber, phase velocity of the waves can be defined as $v_g = c/n(\omega)$ in terms of frequency. Dispersion is generally thought either normal or anomalous dispersion in which the lower frequencies (red-shifted) travel faster than higher frequencies (blue shifted) or vice verse, respectively. Since each frequency component travels at different speed, the wave starts to broaden.

The effect of GVD on the pulse propagation in a linear medium can be studied by eliminating all the nonlinear terms in Schrödinger equation. [5] Then the NLS equation is simplified as;

$$i\frac{\partial A}{\partial z} = -\frac{\beta_2}{2}\frac{\partial^2 A}{\partial t^2} \tag{1.2}$$

This differential equation is easily solved by Fourier transform method. The normalized pulse of arbitrary shape in time domain $A(z,t)$ and its spectrum $\hat{A}(z,\omega)$ in frequency domain are related by Fourier transform as:

$$A(z,t) = \frac{1}{2\pi}\int_{-\infty}^{\infty}\hat{A}(z,\omega)\exp(-i\omega t)d\omega \tag{1.3}$$

By taking the Fourier transform of both sides and using the relevant property of $\frac{\partial^2}{\partial t^2} \to (iw)^2$, equation (1.1) transforms into an ordinary differential equation;

$$i\frac{\partial \hat{A}}{\partial z} = -\frac{1}{2}\beta_2\omega^2\hat{A} \tag{1.4}$$

with having a solution of:

$$\hat{A}(z,\omega) = \hat{A}(0,\omega)\exp\left(\frac{i}{2}\beta_2\omega^2 z\right) \tag{1.5}$$

By looking at the solution, it is seen that GVD changes the phase of initial pulse spectrum by adding phase to each component proportional to its frequency and propagation length. This phase change in spectrum modifies the pulse shape in time domain. [5] The corresponding time domain solution is evaluated by substituting equation (1.5) into equation (1.3).

$$A(z,t) = \frac{1}{2\pi}\int_{-\infty}^{\infty}\hat{A}(0,\omega)\exp\left(\frac{i}{2}\beta_2\omega^2 z\right)\exp(-i\omega t)d\omega \tag{1.6}$$

In the simulations, Gaussian pulses are used as an initial pump pulse. Thus, the effect of GVD on the Gaussian pulses can be summarized in following equations.

Initial pulse is defined by a normalized Gaussian pulse having amplitude of unity as: [5]

$$A(0,t) = \exp\left(\frac{(1+iC)}{2}\left(\frac{t}{T_0}\right)^2\right) \tag{1.7}$$

where C is the initial chirp parameter and T_0 is the half width at 1/e intensity point and related to full width at half maximum as $T_{FWHM} = 1.665\,T_0$. The final pulse after propagation becomes:

$$A(z,t) = \frac{T_0}{\sqrt{T_0^2 - i\beta_2 z(1+iC)}}\exp\left(-\frac{(1+iC)t^2}{2(T_0^2 - i\beta_2 z(1+iC))}\right) \tag{1.8}$$

It is easily seen that both unchirped (C=0) and chirped ($C \neq 0$) Gaussian pulses preserve their shapes after propagation. However, the pulse width T_1 (defined similar to T_0) and the chirp parameter C_1 of the final pulse changes due to GVD as: [5]

$$\frac{T_1}{T_0} = \left[(1 + \frac{C\beta_2 z}{T_0^2})^2 + (\frac{\beta_2 z}{T_0^2}) \right]^{1/2} \tag{1.9}$$

$$C_1(z) = C + (1 + C^2)\frac{\beta^2 z}{T_0^2} \tag{1.10}$$

According to the results, it is obvious that initial pulse starts to broaden due to GVD independent of whether the medium is normal $(\beta_2 > 0)$ or anomalous $(\beta_2 < 0)$ if there is no initial chirp on the pulse. If there is an initial chirp and $\beta_2 C > 0$, pulse broadens at a rate faster than unchirped pulse. However, if $\beta_2 C < 0$, then the pulse drastically starts to compress to compensate the effect of initial chirp and then starts to broaden again. [5]

Simulation Results

The following simulation results show the GVD effect on the Gaussian pulse in time and frequency domain. These results obtained by using Split Step Fourier Method perfectly match with the theory and the experimental results which have proposed by other groups.

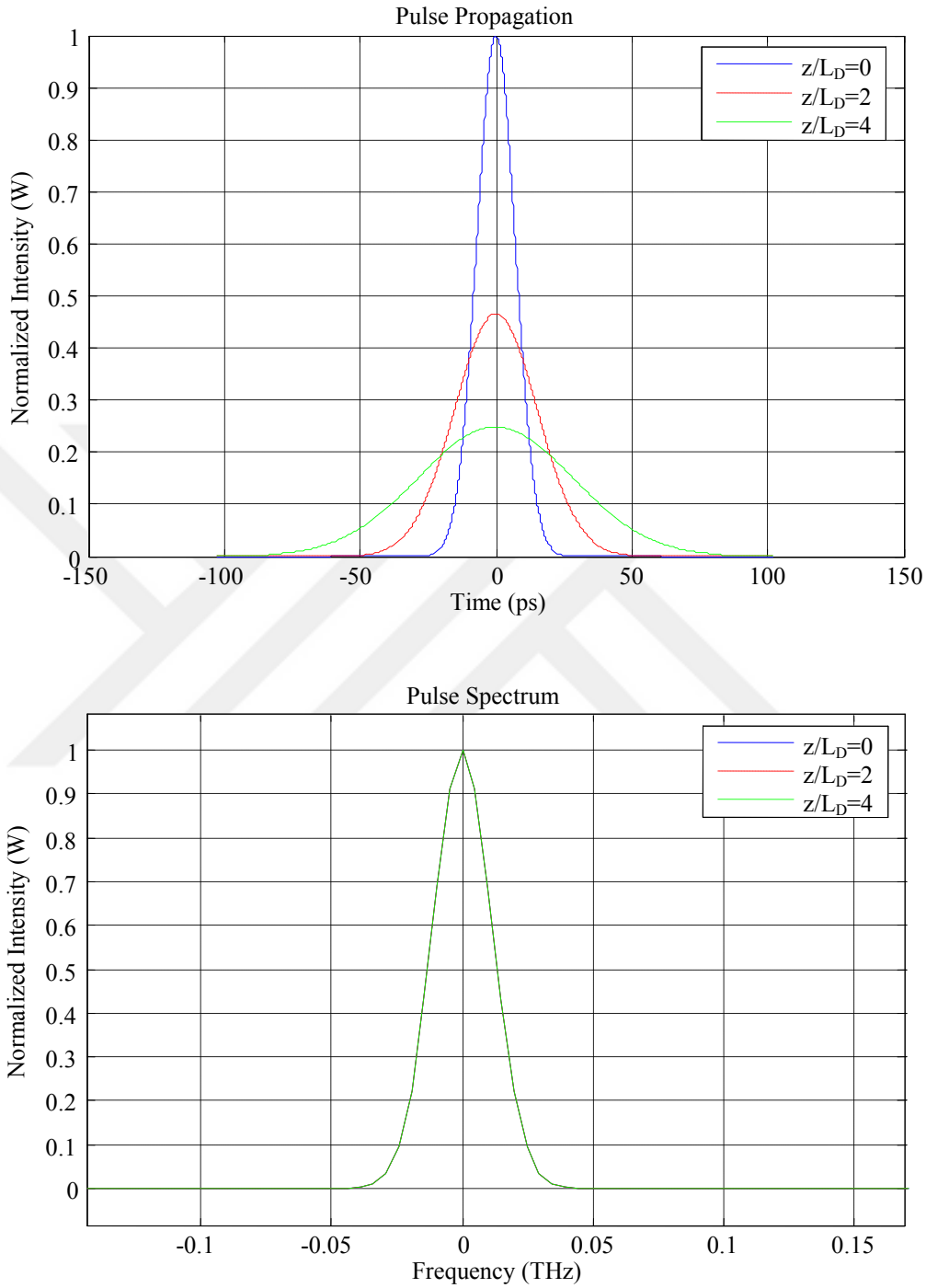

Fig. 1.1 Transform limited Gaussian pulse propagation in a fiber. Temporal (upper) and Spectral (down) evolution due to GVD (D=18 ps/km-nm).

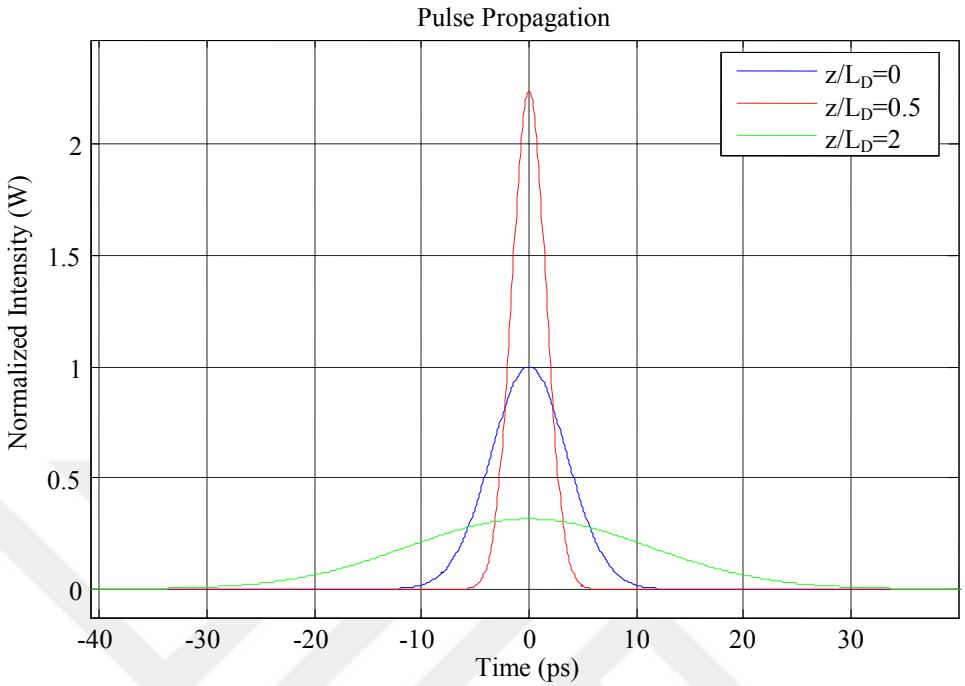

Fig.1.2 Chirped Gaussian pulse (C=2) propagation in a fiber under the effect of GVD ($\beta_2 = -22.9\ ps^2/km$). $L_D = \frac{T_0^2}{|\beta_2|}$ is the dispersion length.

1.2 Nonlinear Optical Effects

When the intensity of electromagnetic field (laser) increases due to small core area of the fiber and high peak power of the ultra short pulses, the optical medium response becomes nonlinear. Two basic nonlinear effects are Self Phase Modulation (SPM) and Cross Phase Modulation (XPM). [5]

1.2.1 Self Phase Modulation

Refractive index of the dielectric medium is not only dependent to frequency but also it is dependent to intensity. When the intensity of light inside the medium increases, the index profile becomes nonlinear. As a result, the pulse experiences both GVD and nonlinear

effects while propagating in fiber. The dominant effect, however, is directly related with the comparison between the dispersion length $L_D = \frac{T_0^2}{|\beta_2|}$ and the nonlinear length $L_{NL} = \frac{1}{\gamma P_0}$ where γ is the nonlinearity parameter and P_0 is the peak power of the pulse. [5] There are three different scenarios as:

i) If $L>L_D$ and $L>L_{NL}$ both GVD and SPM is effective.

ii) If $L_D>>L>L_{NL}$ then GVD is negligible.

iii) If $L_{NL}>>L>L_D$ then SPM is negligible.

Thus, the individual effect of SPM can be studied by eliminating the GVD, assuming the second scenario, in NLS equation as:

$$\frac{\partial A}{\partial z} = ie^{-az}\gamma P_0 |A|^2 A \tag{1.11}$$

According to this equation, it is seen that the SPM induces an intensity dependent nonlinear phase on the pulse without changing the pulse shape in time domain. The solution to this ordinary differential equation is simply,

$$A(z=L,t) = A(0,t)\exp[i\phi_{NL}(z=L,t)] \tag{1.12}$$

where $\phi_{NL}(L,t) = |A(0,t)|^2 \gamma P_0 L_{eff}$ is the nonlinear phase and $L_{eff} = \frac{[1-\exp(-\alpha L)]}{\alpha}$ is the effective length. The maximum phase shift occurs at the center of the pulse, namely at the peak intensity point which is given by $\phi_{\max} = \gamma P_0 L_{eff}$.

Due to Fourier theorem, any time dependent phase on the signal generates new frequency components in frequency domain. In other words, temporally changing phase across the pulse makes the instantaneous frequency deviates from its center value w_0 causing a spectral broadening. [5] The amount of SPM induced spectral shift, also called frequency chirp (δw) is obtained by taking the derivative of nonlinear phase.

$$\delta\varpi(T) = -\frac{\partial \phi_{NL}}{\partial t} = -\gamma P_0 L_{eff} \frac{\partial}{\partial t}\left|A(0,T)\right|^2 \tag{1.13}$$

For Gaussian pulses the SPM induced frequency shift is:

$$\delta\omega(t) = \frac{2}{T_0^2}\frac{L_{eff}}{L_{NL}} t \exp\left(-\frac{t^2}{T_0^2}\right) \tag{1.14}$$

with a maximum shift of $\delta\omega_{\max} = 0.86\Delta\varpi_0\phi_{\max}$ where $\Delta\varpi_0 = T_0^{-1}$.

Simulation Results

The following simulation results show the SPM effect on the Gaussian pulse in time and frequency domain. While the pulse shape does not change through the propagation, the spectrum is drastically distorted. These results obtained by using Split Step Fourier Method perfectly match with the theory and the experimental results which have already proposed by other groups.

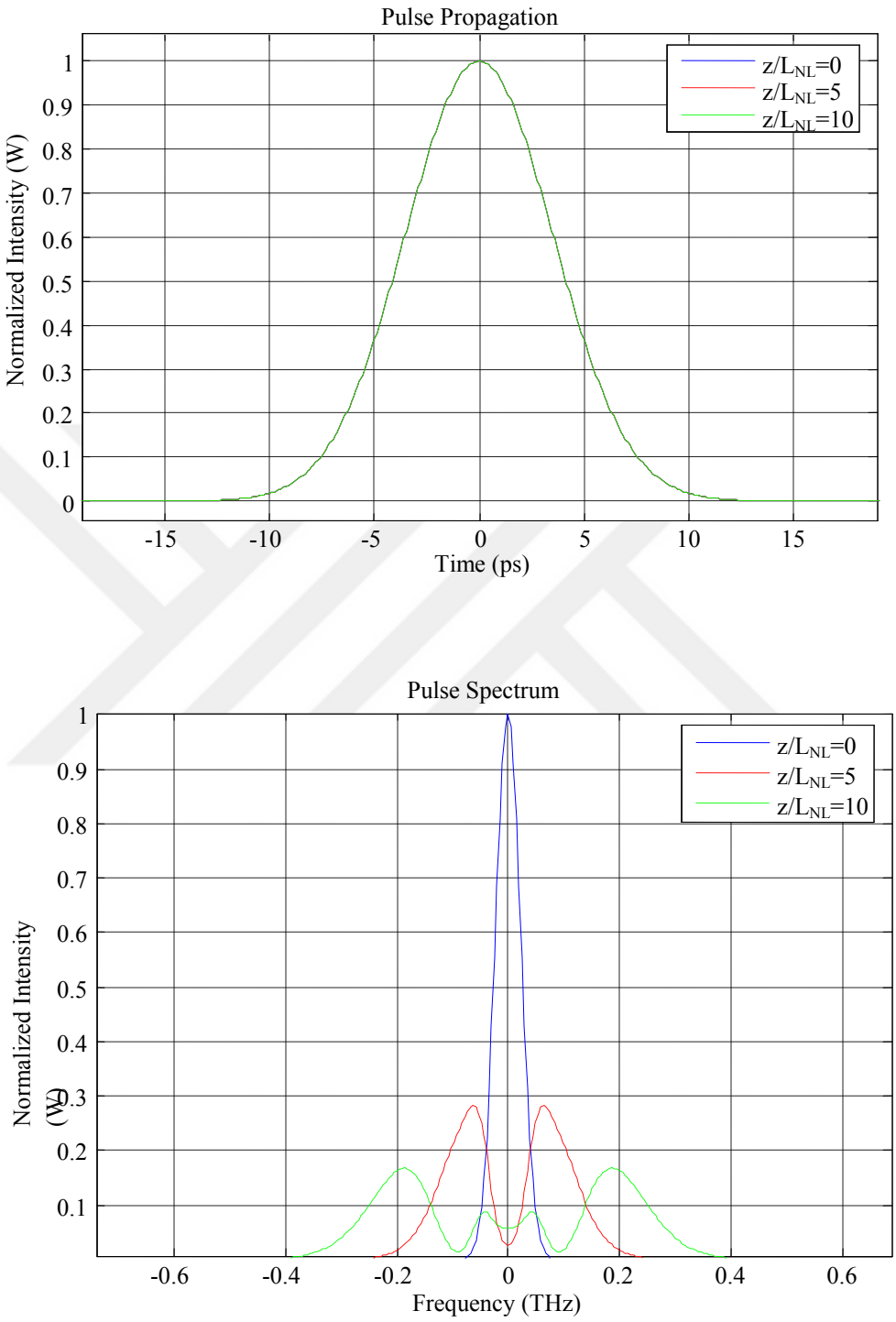

Fig.1.3 Transform limited Gaussian pulse propagation inside the fiber. Temporal (upper) and Spectral (down) evolution due to nonlinear effect ($\gamma = 2\ W^{-1}km^{-1}$).

1.2.2 Cross Phase Modulation (XPM)

XPM is another nonlinear phenomenon that causes spectral broadening of the pulses when two or more optical beams having different carrier frequencies are simultaneously launched into a medium. When they interact with each other by inducing an additional nonlinear phase, each optical beam experiences a refractive index which is not only affected by the intensity of that beam but also the intensity of other beams. [5] Their effect on each other through XPM is actually two times more effective than SPM for the same intensity.

To summarize, in a medium where N optical pulses with different frequencies propagate simultaneously, the total nonlinear phase seen by each pulse due to SPM and XPM becomes;

$$\phi_j(t) = \gamma_j \left[L\left|A_j(0,t)\right|^2 + 2\sum_{j\neq k}\int_0^L \left|A_k(0,t-zd)\right|^2 dz \right] \tag{1.15}$$

where $j = 1-N$. Time dependence of the nonlinear phase due to XPM also implies an additional frequency shift δw in frequency domain.

As seen in the equation (1.15), XPM is also dependent to the relative positions of the pulses. Since the pulses travel at different velocities in a dispersive medium, they only overlap in a certain time window. The walk-off between the pulses affects the spectral changes and broadening due to XPM. [7]

1.3 Numerical Solutions to Nonlinear Schrödinger Equation

In general, there is no analytical solution to full wave Maxwell equation for nonlinear optical medium. Numerical solutions on the other hand, because of dimensionality problem are very difficult to apply. However, an approximate solution can be obtained due to some predefined conditions and assumptions. There are basically two kinds of numerical methods as pseudo spectral and finite difference methods. The main difference between them is the elimination of carrier frequency. Because the finite difference methods involve the carrier frequency, they can account for forward and backward propagating waves with more accurately than SSFM. [21]

Split Step Fourier Method (SSFM) is one of the pseudo-spectral numerical methods which is easier to implement and computationally faster compared to other numerical methods. SSFM has been an extensively used numerical method aims to solve NLS equation for the propagation of pulses. [5]

Split Step Fourier Method (SSFM)

The basic principle behind the SSFM is that it tries to solve the NLS equation as combination of linear and nonlinear terms by treating each part separately. Both linear and nonlinear parts have analytical solutions but NLS equation including both parts does not have an analytical solution. Thus, by dividing the propagation distance into small steps (h), two parts can be solved separately with a small numerical error. Briefly, the

linear term due to dispersion and nonlinear term due to nonlinear optical effects are defined respectively as;

$$D = -\frac{\alpha}{2} - \sum_{m=2} \frac{i^{m-1}}{2^{m-1}} \beta_m \frac{\partial^m}{\partial T^m} \tag{1.16}$$

$$N = i\gamma \left[|A(z,t)|^2 + \frac{2i}{\varpi_0 A(z,t)} \frac{\partial}{\partial t} [|A(z,t)|^2 A(z,t)] \right]$$

where $A(z,t)$ is the complex field envelope at distance (z) and time (t). Thus the NLS equation can be written in the form as: [5]

$$\frac{\partial A(z,t)}{\partial z} = (D+N)A(z,t) \tag{1.17}$$

with a general solution of

$$A(z+h,t) = \exp[h(D+N)]A(z,t). \tag{1.18}$$

The solution to this partial differential equation is approximated by propagating the optical fields over small distance (h) where the dispersive and nonlinear effects are assumed to act independently. In other words, propagation from z to z+h can be held in two steps in which dispersion and nonlinearity acts alone. [5]

$$\exp[h(D+N)] \approx \exp[hD]\exp[hN] \tag{1.19}$$

The dispersion (D) effect is analyzed in frequency domain rather than taking derivative in time domain to reduce the computational time. Thus, taking the Fourier Transform of

both sides and using the Fourier transform property $\frac{\partial^2}{\partial T^m} \to (iw)^m$ derivative with respect to time transforms to multiplicative operators and NLS equation reduces to:

$$\frac{\partial A(z,\varpi)}{\partial z} = -\frac{\alpha}{2} - \sum_{m=2} \frac{i^{m-1}}{2^{m-1}} \beta_m (i\varpi)^m A(z,\varpi) \tag{1.20}$$

with the solution of,

$$A(z+h,\varpi) = A(z,\varpi) \exp\left[h\left[-\frac{\alpha}{2} - \sum_{m=2} \frac{i^{m-1}}{2^{m-1}} \beta_m (i\varpi)^m \right]\right]$$

and

$$A(z+h,t) = \Im^{-1}\{A(z+h,\varpi)\}. \tag{1.21}$$

To reduce the error accumulation more, a new version of SSFM called symmetrized SSFM is used in simulations. The general procedure applied in symmetrized SSFM at every h distance is as follows;

1. Dispersion and loss is calculated over h/2 by setting N=0.

$$A(z+\frac{h}{2},T) = \Im^{-1}\left\{ \exp\left[\frac{h}{2} D(i\varpi) \right] \Im\{A(z,T)\} \right\}.$$

2. At the midpoint of step size, nonlinearity is calculated by setting D=0.

$$A(z+\frac{h}{2},T) = A(z+\frac{h}{2},T) \exp(hN).$$

3. Dispersion and loss is calculated over the second half by setting N=0.

$$A(z+h,t)=\Im^{-1}\left\{\exp\left[\frac{h}{2}D(i\varpi)\right]\Im\left\{A(z+\frac{h}{2},t)\right\}\right\}.$$

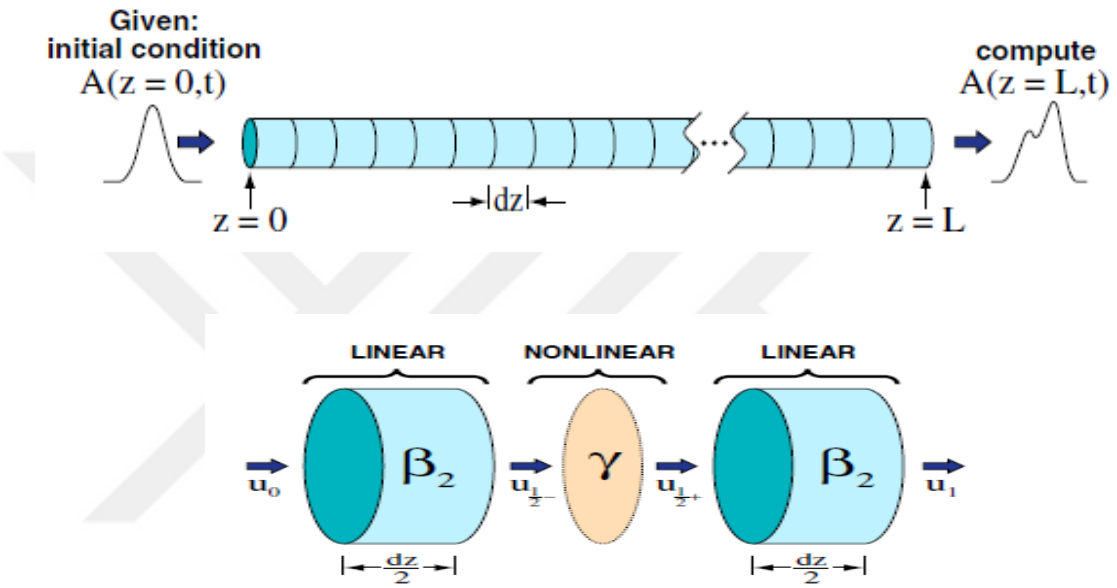

Fig.1.4 Schematics of Split Step Fourier Method. [17]

1.4 Stimulated Raman Scattering (SRS)

Stimulated Raman Scattering is another non-linear process that occurs in any molecular medium. Raman scattering in fibers have been widely utilized to operate optical fibers as an amplifier or tunable laser by transferring energy from one beam (Pump) to others (Stokes). [5]-[9] In other words, the weak low frequency probe beam, also called Stokes wave, is amplified by the intense higher frequency pump beam trough SRS process. The

amount of energy transferred from incident field to scattered field is determined by the vibrational modes of the medium. [8]

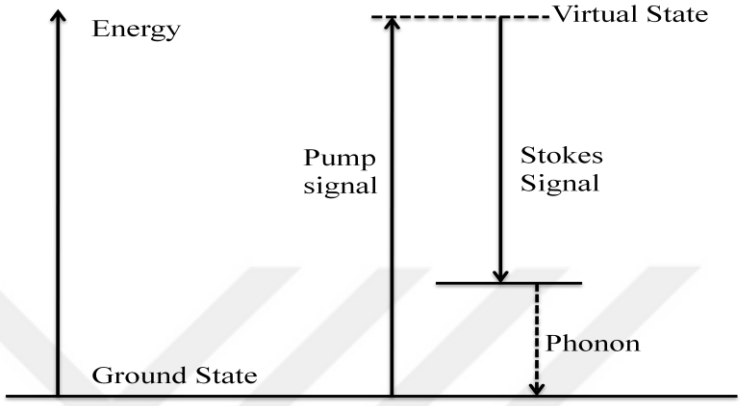

Fig. 1.5 Energy Diagram of Raman Scattering.

Briefly, the initial growth of the Stokes wave is governed by the following formula.

$$\frac{\partial I_s}{\partial z} = g_R I_p I_s \tag{1.22}$$

where I_p is the pump intensity, I_s is the initial Stokes intensity and g_R is the Raman gain coefficient.[10] Raman gain coefficient is a function of frequency shift $(\Omega = \omega_p - \omega_s)$ between the pump and Stokes waves, and generally depends on the composition of the fiber core, relative polarization of both fields (co-polarized or orthogonally polarized) and the pump wavelength (inversely proportional). [11] The Raman gain in silica fibers has a very broad spectrum (up to 40THz) with the first peak at nearly 13.2THz and the second peak at 14.7THz due to non-crystalline nature of silica glass. [12] Raman induced frequency shift enables to generate 26.4-29.4THz (~1000cm^{-1}) frequency separated second order Stokes pulses with ~3THz (~40nm) tunability. This impressive property of

Raman laser enables to design multi wavelength stable soliton pulses to be used in many applications.

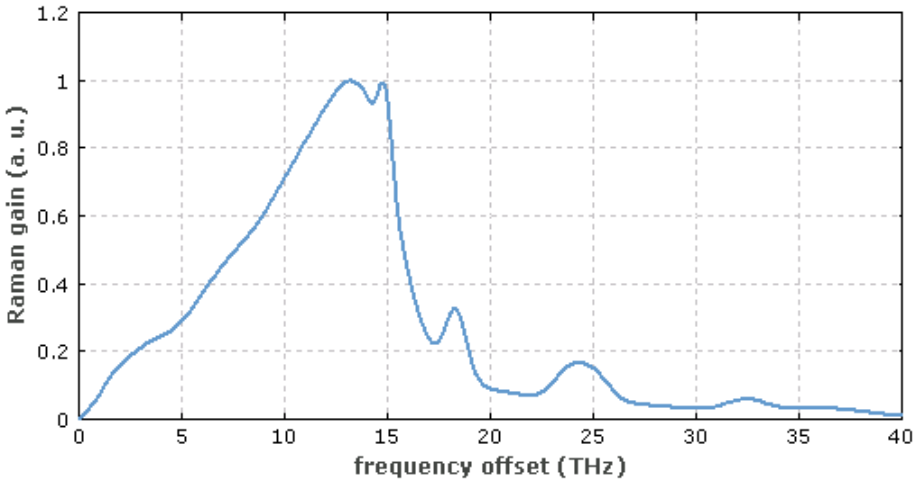

Fig.1.6 Raman Gain spectrum of silica fiber. [13]

As shown in the Figure 1.6, Raman gain spectra shows a multi-peak structure due to contribution of many vibrational modes. Although all the fine structures will be absent, Raman gain spectra can simply be modeled by a single peaked function like polynomial, Gaussian or Lorentzian. [13]

Stimulated Raman Scattering, briefly, occurs when both pump and probe (Stokes wave) beams simultaneously propagate inside a fiber. The probe beam starts to be amplified due to Raman induced energy transfer from pump beam, as long as the frequency shift lies within the bandwidth of gain spectra. Even without an initial probe beam, by spontaneous Raman scattering new frequency components are generated and amplified through the propagation. Although spontaneous Raman scattering generates photons within the entire bandwidth and all are amplified, the frequency component where the Raman gain is maximum is amplified more and dominates in the system. As a

result, Stokes wave with a frequency determined by the Raman peak gain (nearly 13.2 THz downshifted for silica) is generated by the SRS.

For the simplest case in which the CW pump beam is launched inside a fiber, the evolution of pump and the probe beams is governed by the following equations including both the fiber losses and the interaction between them through SRS process. [5]

$$\begin{aligned}\frac{\partial I_s}{\partial z} &= g_R I_p I_s - \alpha_s I_s \\ \frac{\partial I_p}{\partial z} &= -\frac{\omega_p}{\omega_s} g_R I_p I_s - \alpha_p I_p\end{aligned} \tag{1.23}$$

where α_p and α_s are the fiber loss coefficients for pump and Stokes frequencies. As seen in the SRS equation, the term $\frac{\omega_p}{\omega_s} > 1$ indicates that the energy emitted from the pump beam is more than the energy gained by the Stokes beam. The remaining energy is lost as phonons in the systems.

There is no analytical solution for these differential equations. However, for the small signal case, i.e. signal is much weaker than the pump, the pump depletion due to the amplification process can be neglected (first term in the second equation) and hence the solution becomes:

$$I_s(z = L) = I_s(0) \exp(g_R I_0 L_{eff} - \alpha_s L) \tag{1.24}$$

where I_0 is the incident pump intensity and L is the propagation length. In order for the Stokes wave to build up in the fiber, the gain should be greater than the loss as verified in the solution. This solution can only be applied for the initial stages of Raman Soliton

generation. Stokes wave circulates in a cavity and is amplified rapidly to reach a steady state by depleting the pump. Thus, for the lasing of the Stokes wave, pump depletion cannot be ignored.

1.5 Optical Solitons

Soliton as its name implies, is a particle like wave propagating in a nonlinear medium preserving its shape and surviving after collisions. Propagating undistorted is the most impressive feature of Soliton that enables them to be used in long-haul optical communication systems. [6]

Soliton wave is basically the result of interplay between GVD and SPM which independently affect the propagating pulse in a fiber. GVD as discussed in detail is a linear dispersive effect which broadens the optical pulse unless it is initially chirped. In other words, if the pulse is not transform-limited and chirped in a way that the chirp parameter (C) and the GVD parameter β_2 have opposite signs, the pulse compresses during the early stages of propagation and starts to broaden again. On the other hand, SPM as a dominant nonlinear effect introduces a positive chirp (C>0) on the propagating pulse. As a result, when the GVD parameter $\beta_2 < 0$ is negative, namely the pulse propagates in anomalous regime; the broadening effect of GVD can be totally balanced by SPM induced chirp mainly in the central part of the pulse. More specifically, since the SPM induced chirp can be adjusted by tuning the power properly, it cancels the negative chirp induced by GVD. [6] The basic physics under the Soliton wave is explained as in anomalous regime the lower frequency components travel faster than the high frequency components as a result of GVD. SPM, however, affects the pulse in a way that the high

frequencies are moved to the leading edge and low ones to the tailing edge, namely induces a positive chirp. As a result of such corporation, total chirp on the pulse is cancelled and enables an undistorted propagation. Briefly, Soliton is a solution of nonlinear Schrödinger equation including both SPM and GVD effects as:

$$\frac{\partial A}{\partial z} + i\frac{\beta_2}{2}\frac{\partial^2 A}{\partial t^2} = i\gamma|A|^2 A \tag{1.25}$$

By introducing $\tau = \frac{t}{T_0}$, $\xi = \frac{z}{L_D}$ and $U = \frac{A}{\sqrt{P_0}}$ where T_0 is the measure of pulse width, P_0 is the peak power of the pulse and $L_D = \frac{T_0^2}{|\beta_2|}$ is the dispersion length. [5] The equation (1.25) normalizes to:

$$i\frac{\partial U}{\partial \xi} - \frac{s}{2}\frac{\partial^2 U}{\partial \tau^2} + N^2|U|^2 U = 0 \tag{1.26}$$

where $s = \mathrm{sgn}(\beta_2)$ is the sign of β_2 and the $N^2 = \gamma P_0 L_D = \gamma P_0 \frac{T_0^2}{|\beta_2|}$ represents the dimensionless parameter related with the Soliton order. Also, by defining $u = NU$ and setting $s = -1$ (propagating in an anomalous dispersion regime) the final form of the NLS equation becomes

$$i\frac{\partial u}{\partial \xi} + \frac{1}{2}\frac{\partial^2 u}{\partial \tau^2} + |u|^2 u = 0 \tag{1.27}$$

which is a special class of nonlinear differential equations that can be solved by inverse scattering method. This equation supports the Soliton wave solution. According to this normalized NLS equation, when the input pulse having an initial envelope of

$u(0,\tau) = N\sec h(N\tau)$ is launched into the fiber, it either preserves its shape and remains undistorted or repeats its shape periodically at every $\xi = m\frac{\pi}{2}$ distance. [5]

As a result, the parameter N determines the propagation pattern of the pulse. If N=1 which means the fundamental soliton case, pulse propagate without changing its shape. However, if N>1 which means high-order soliton case, pulse follows a periodic pattern. The physical meaning behind the parameter N is hided in its definition of $N^2 = \frac{L_D}{L_{NL}}$. N can be thought as the comparison between the dispersion and the nonlinear lengths where only GVD and SPM dominate, respectively.

Soliton Propagation and Simulation Results

Soliton propagation inside a lossless fiber is analyzed for different soliton-order cases. In order to test the reliability of our simulation program, the results are compared with the theoretical ones. For simplicity, we analyzed only the first, second and the third order Soliton propagation.

In the first case, we analyzed the propagation of first order, namely the fundamental soliton pulse. As seen in the following figure, the fundamental soliton whose the pulse width and the peak power is chosen to satisfy N=1, preserves its shape along the propagation inside the lossless fiber.

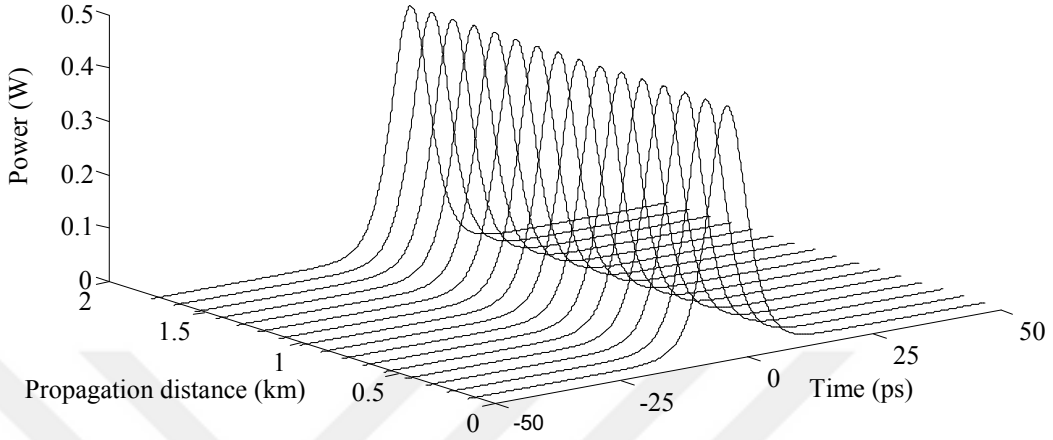

Fig.1.7 Fundamental Soliton pulse evolution in a fiber.

In the following figure, it is seen that the pulse width remains same along the propagation. Pulses at initial, half-soliton period and soliton period positions are also extracted to show that pulse shape remains undistorted.

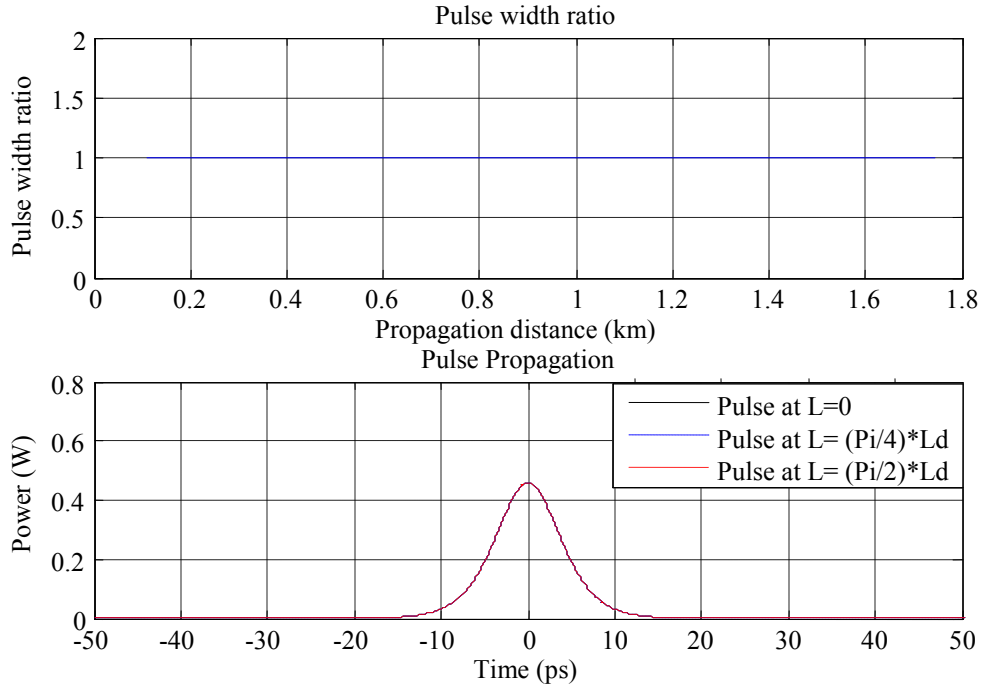

Fig.1.8 Ratio of the pulse width of final pulse to the initial pulse (up), pulses at L=0 $L=z_0/2$ and $L=z_0$.

However, for the higher-order soliton case, the situation is completely different. Soliton pulses chosen such that N>1, propagate by changing their shapes, pulse widths and peak powers periodically. In fact, this periodicity occurs for all higher-order solitons. At every $\xi = m\frac{\pi}{2}$ distance, soliton recovers its original shape. This pattern is repeated over each section of soliton period which is defined as $z_0 = \frac{\pi}{2} L_D$.

For the second order case, as seen in the following figures, soliton contracts to a fraction of its initial pulse width and merges again to its original shape.

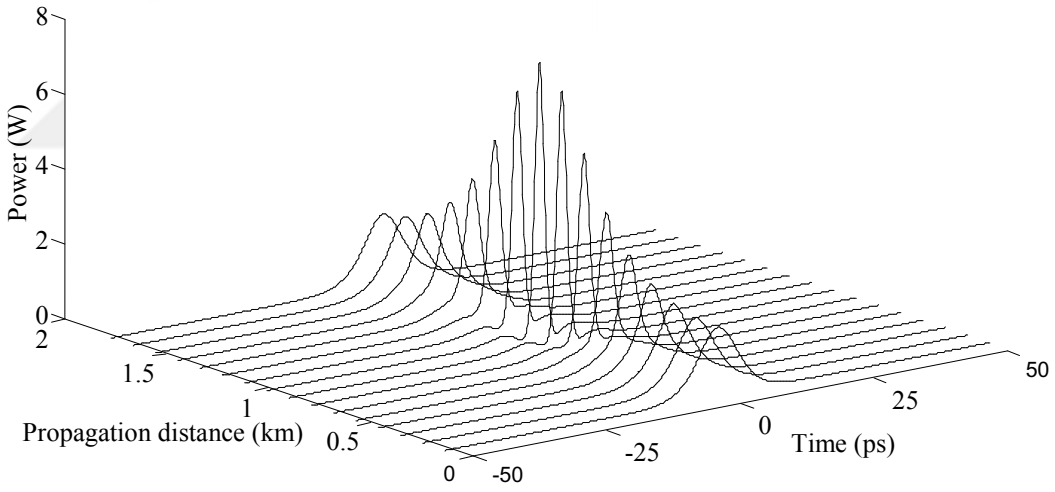

Figure 1.9 Second order Soliton pulse evolution in a fiber.

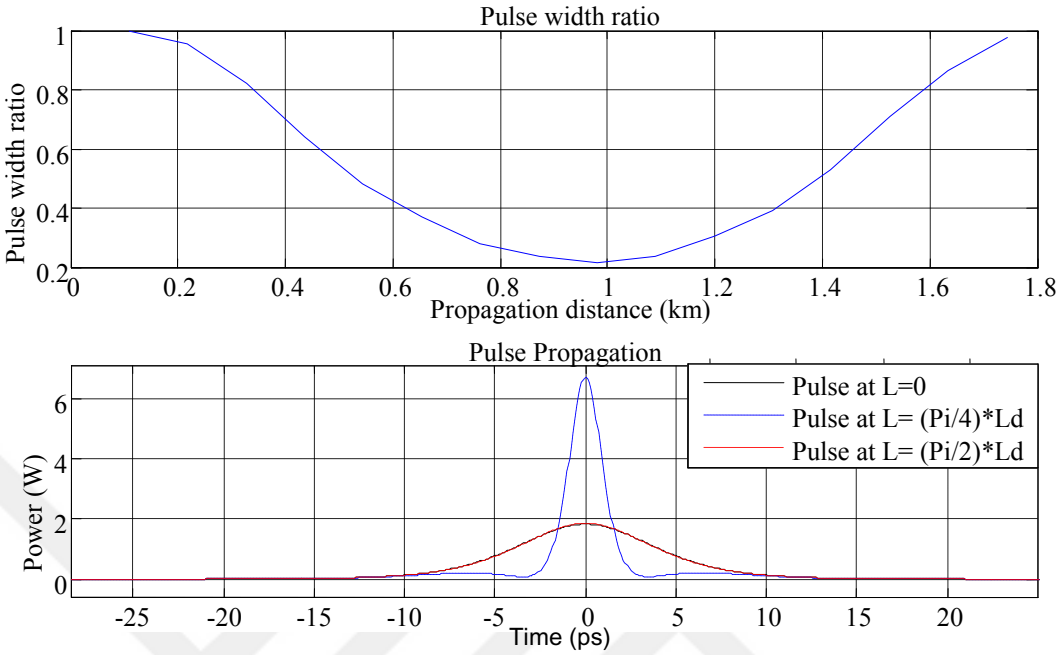

Fig.1.10 Ratio of the pulse width of final pulse to the initial pulse (up), pulses at L=0 $L=z_0/2$ and $L=z_0$.

For the third order case, as seen in the following figures, soliton first compresses, splits into two distinct pulses at the half period and merges again to its original shape.

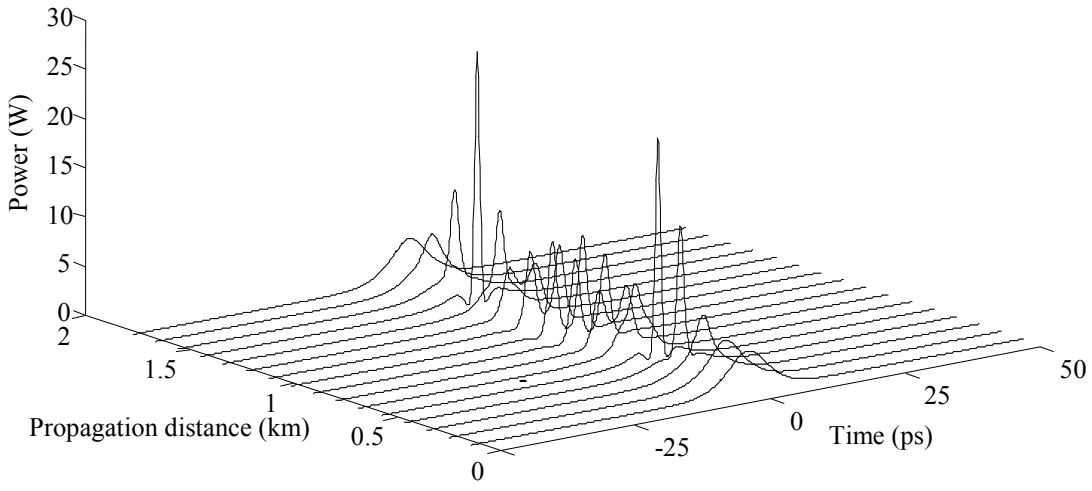

Fig. 1.11 Third order Soliton pulse evolution in a fiber.

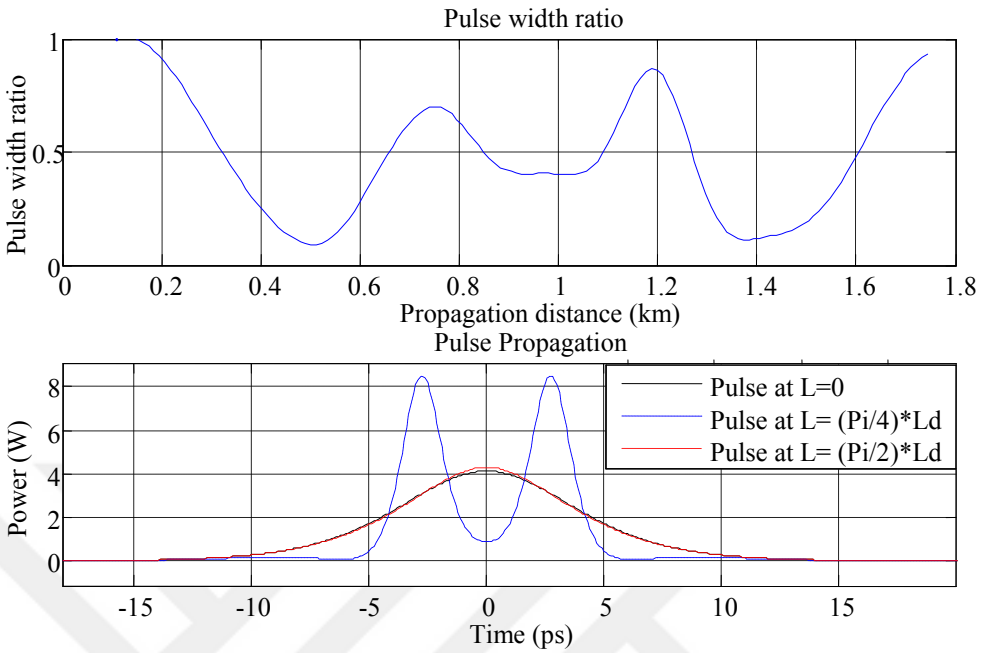

Fig.1.12 Ratio of the pulse width of final pulse to the initial pulse (up), pulses at L=0 $L=z_0/2$ and $L=z_0$.

1.5.2 Perturbation of Soliton

Soliton pulses propagate by retaining their shapes in a fiber where only the GVD and SPM effects are included. However, for the fiber Raman Soliton laser experiment such other impacts of fiber losses and stimulated Raman scattering should be included in NLS equation. Thus, these effects can be treated in Soliton propagation equation as small perturbations. Perturbed NLS can be considered as:

$$i\frac{\partial u}{\partial \xi}+\frac{1}{2}\frac{\partial^2 u}{\partial \tau^2}+|u|^2 u = i\varepsilon(u) \tag{1.28}$$

where $\varepsilon(u)$ represents the small perturbation that is a function of u. [5] This equation can only be solved for small perturbation by assuming the functional form of Soliton solution remains same but having different parameters. Thus the solution for perturbed NLS equation becomes:

$$u(\xi,t)=\eta(\xi)\sec h[\eta(\xi)(\tau-q(\xi))]\exp[i\phi(\xi)-i\delta(\xi)\tau] \tag{1.29}$$

where η,δ,q,ϕ are defined as the amplitude, frequency, position and the phase parameters of the Soliton which all depend on the propagation distance. The impact of the perturbation results in a change of these Soliton parameters. The evolution of these four parameters due to the perturbation can be solved by using variational method. To determine the final values of parameter set, the following equations are required to be solved:

$$\begin{aligned}
&\frac{d\eta}{d\xi}=\mathrm{Re}\int_{-\infty}^{\infty}\varepsilon(u)u^{*}(\tau)d\tau,\\
&\frac{d\eta}{d\xi}=-\mathrm{Im}\int_{-\infty}^{\infty}\varepsilon(u)\tanh[\eta(\tau-q)]u^{*}(\tau)d\tau,\\
&\frac{d\eta}{d\xi}=-\delta+\frac{1}{\eta^{2}}\int_{-\infty}^{\infty}\varepsilon(u)(\tau-q)u^{*}(\tau)d\tau,\\
&\frac{d\eta}{d\xi}=\mathrm{Im}\int_{-\infty}^{\infty}\varepsilon(u)\left\{\frac{1}{\eta}-(\tau-q)\tanh[\eta(\tau-q)]\right\}u^{*}(\tau)d\tau+\frac{1}{2}(\eta^{2}-\delta^{2})+q\frac{d\delta}{d\xi}
\end{aligned} \tag{1.30}$$

where Re and Im stands for the real and imaginary parts respectively. [14]

a) Fiber Loss as a Perturbation

Soliton preserves its shape as a result of balance between GVD and SPM effects. However, if the fiber loss is accounted, the peak power of the Soliton decreases with the length reducing the effect of SPM. Since the Soliton dissipates the perturbation to preserve its shape, it adjusts its pulse width accordingly. To balance the reduction in SPM effect, Soliton reduces GVD effect by increasing its pulse width. The fiber losses can be treated as $i\varepsilon(u)=-\frac{i}{2}\Gamma u$ where $\Gamma=\alpha L_{D}$ and the analytical solution by integrating the

equations in (1.23) shows that only the amplitude and phase parameters are affected by fiber losses.

$$\eta(\varepsilon) = \eta(0)\exp(-\Gamma\xi) \qquad \phi(\xi) = \phi(0) + \frac{[1-\exp(-2\Gamma\xi)]}{4\Gamma} \tag{1.31}$$

Since the pulse width T_0 is inversely proportional to the amplitude $\eta(\varepsilon)$, the final pulse width becomes $T_1 = T_0 \exp(-\Gamma\xi)$. [15]

b) Soliton Amplification as a Perturbation

Soliton amplification can also be treated as a kind of perturbation on soliton pulses. Basically, there are such two different approaches for soliton amplification as lumped and distributed amplification. [16] In the lumped case, which is mainly used for long-haul communication systems to compensate the fiber losses due arbitrarily long distances, soliton pulses are amplified abruptly after propagating certain distance. Soliton pulses start to adjust themselves to maintain their initial shape by dispersing some energy. If the period of amplification L_A, namely the distance between successive amplifiers, is comparable to the dispersion length L_D, soliton pulses responds to this perturbation by releasing the extra energy as dispersive waves. Thus, the amplification length should be much less than the dispersion length, $L_A << L_D$, to prevent soliton pulses to break up. [6]

On the other hand, for our fiber Raman Soliton laser case, where the stimulated Raman scattering acts as a source of amplification, solitons are amplified adiabatically along the fiber. Since the amplification is distributed over the entire length and there is no abrupt gain, dispersive waves are almost eliminated.

In order to eliminate pulse break up completely even for distributed case, the amplification should be small enough to allow soliton pulse to readjust its parameters along the propagation. Thus, to generate Stokes pulses, the pump power should be selected in the close vicinity of threshold power.

CHAPTER 2

FIRST ORDER RAMAN SOLITON LASERS AND STABILITY ANALYSIS

Fiber Raman Soliton Laser is a new kind of laser that provides an output in the form of soliton with sub-picoseconds widths at the first order Stokes wavelength and it is downshifted by 13.2 THz-14.7 THz. [5] This Raman Soliton lasers mostly include two fiber sections as gain and pulse shaping fibers in a ring cavity configuration. They can also be reduced to a single fiber if the pulse shaping is introduced in the gain fiber [18]. The laser uses the Raman effect to provide gain for the Stokes signal and facilitate lasing. While the pump pulse is circulating inside the cavity, the first order Stokes pulse can be excited. If the required pumping level is satisfied to reach the threshold, Stokes pulse builds up in the cavity and acquires the proper energy to converge to a fundamental soliton with much shorter pulse width.

To assess the conditions where first order solitons can be generated we developed a numerical and analytical formula that includes the nonlinear and linear effects of fibers and interactions between pump lasers and Stokes signals at the first order. The mutual interaction between the pump pulse and the Stokes pulse inside the cavity is governed by a set of two non-linear Schrodinger equations including all processes of GVD, SPM, XPM, walk off between the pulses, Raman gain and pump depletion as: [5]

$$\frac{\partial A_p}{\partial z}+\frac{1}{v_{gp}}\frac{\partial A_p}{\partial t}+i\frac{\beta_{2p}}{2}\frac{\partial^2 A_p}{\partial t^2}+\frac{\alpha_p}{2}A_p=i\gamma_p(|A_p|^2+2|A_s|^2)A_p+R_p(z,t)$$

$$\frac{\partial A_s}{\partial z}+\frac{1}{v_{gs}}\frac{\partial A_s}{\partial t}+i\frac{\beta_{2s}}{2}\frac{\partial^2 A_s}{\partial t^2}+\frac{\alpha_s}{2}A_s=i\gamma_s(|A_s|^2+2|A_p|^2)A_s+R_s(z,t) \quad (2.1)$$

where $v_{gp,gs}$ is the group velocities, $\gamma_{p,s}$ is the nonlinearity coefficients, $\beta_{2p,2s}$ is the GVD parameters and $A_{p,s}$ is the amplitudes of the pump and Stokes signals, respectively. Here, $R_p(z,t)$ generates the depletion of the pump signal and $R_s(z,t)$ is responsible for gain on the Stokes signal due to Raman effect.

SSFM is used to solve these coupled differential equations. In the simulations, transform-limited Gaussian pulses with 10ps (FWHM) pulse width and 5W to 10W peak power, were used as a pump signal. For the pump signal $(\lambda_p=1550nm \ and \ \beta_2\approx-3ps^2/km)$, the dispersion length $L_D=\frac{T_0^2}{|\beta_2|}$ becomes more than 12km and nonlinear length $L_{NL}=\frac{1}{P_0\gamma}$ becomes around 100m (for γ=2W^{-1}km^{-1}). Since the condition $L_D>>l_g>L_{NL}$ is satisfied, GVD effect on the pump pulse in equation (2.1) can be neglected and pump pulse propagation can be treated as in a SPM dominant regime where it is only affected by SPM. Thus, it propagates without changing its shape in time domain except being attenuated due to fiber loss and depletion due to Stokes signal.

However, for the Stokes signal both dispersive and nonlinear effects become important. Stokes pulses evolve from a pre-defined low power DC background through

stimulated Raman amplification. In order for the Stokes pulses to form, the pump power must be greater than the threshold. Threshold power is determined due to the fiber losses, attenuation factor and the output coupling ratio. According to the simulation set up, total distributed loss in which attenuation and coupling factors are treated as distributed loss is calculated by $\alpha_{loss} = \alpha(l_g + l_{sh}) - \ln(CX)$, where α is the fiber loss coefficient, $l_{g,sh}$ are the gain and shaping lengths, respectively, C is the coupling percentage and X is the attenuation factor. Stokes pulses start to be amplified when the pump power exceeds the threshold. However, there is an upper limit to which the pump power can be increased. If the pump power is adjusted far away from the threshold, Stokes pulses cannot converge to a soliton and break up into several pulses immediately. This effect can be easily explained when we treat amplification as a perturbation to the pulse as discussed before. Stokes pulse, while propagating inside the cavity, slowly adjusts its pulse width and peak power to converge to a fundamental soliton. However, if the gain is very large, Stokes pulse cannot adjust itself quickly and starts to disperse additional energy by extracting dispersive waves. In other words, the perturbation, that is the gain for this case, should be small to prevent Stokes pulse to break up. Thus, the operating region of the pump power is limited to the vicinity of threshold power.

2.1 Time-Dependent Gain

While the Stokes pulse is propagating in a ring cavity, it experiences a time and frequency dependent gain due to Raman effect. The time-dependent gain without saturation, namely in small signal operation regime, can be expressed by: [18]

$$\alpha_g(t,z) = \alpha_g^0 \exp\left[-\left(\frac{t-(z/v_{gp} - z/v_{gs})}{\tau_p} \right)^2 \right] \tag{2.2}$$

$$\alpha_g^0 = g_R P_p^0 l_g \tag{2.3}$$

where $g_R\left(\frac{1}{Wkm}\right)$ is the Raman gain coefficient, P_p^0 is the pump peak power and l_g is the gain fiber length. In equation (2.2), it is obvious that the gain has a Gaussian profile exactly same as the square of pump pulse $(|A_p|^2)$. The position dependency $(z/v_{gp} - z/v_{gs})$ of the gain is nothing short of the walk-off effect on the gain. The peak value of the gain is determined by equation (2.3). Raman gain, as seen in the equation, is proportional to pump peak power, Raman gain coefficient and the propagation length. However, since the pump and the Stokes pulses travel at different velocities the actual interaction length decreases which results in less gain.

When the Stokes signal starts to form and be amplified, its intensity becomes comparable with the pump intensity. The gain medium (fiber in our case), however, cannot maintain the same gain for high signal powers. Since the high power signal suddenly reduces the population of excited atoms, the strength of the gain decreases. Gain is directly proportional to the number of excited atoms in the medium. This effect is called the saturation phenomenon, which must be included in simulations. There are actually two such kinds of mechanisms as homogeneous and inhomogeneous broadening which saturation shows up. In homogeneous broadening case, since all emitters (excited atoms) responds in a same manner, namely has a same emission spectrum, the spectral

shape does not change. The energy to amplify the Stokes signal is supplied by all the atoms making the whole line shape of gain profile decreases. On the other hand, for in homogeneously broadened system, since each emitter has different emission profile and responds individually, saturation in the gain line shape shows up locally by causing hole burning in spectrum. For the simulation of Fiber Raman Soliton Laser, the fiber medium is assumed as a homogeneously broadened system. The saturation effect, as a result, can be shown as;

$$P_p = P_p \exp\left(-g_R^{"}\left|A_s^0\right|^2 l_g\right) \approx P_p \frac{1}{1+\frac{\left|A_s^0\right|^2}{P_{sat}}}$$

$$P_{sat} = \frac{1}{g_R^{"} l_g} \quad and \quad g_R^{"} = \left(\frac{w_p}{w_s}\right) g_R \quad and \quad \left|A_s^0\right|^2 = Peak\ signal\ power \tag{2.4}$$

In this equation, the term $\left|A_s^0\right|^2$ (peak power of the Stokes signal) rather than the time-varying envelope, implies that the pump depletion is applied by attenuating the whole line shape as defined by homogeneous broadening. [18] The term inside the exponential is much less than unity, thus we can use Taylor series approximation ($e^{-x} \approx \frac{1}{1+x}$). Also the term $g_R^{"} = \left(\frac{w_p}{w_s}\right) g_R$ is the Raman gain coefficient for the pump signal. The reason why $g_R^{"} > g_R$ is the energy conversion from pump to Stokes pulse being not %100 efficient, in other words, some of the emitted energy is lost in the form of phonons.

Another factor that must be included in gain calculation is the frequency dependency of stimulated Raman scattering. As discussed before, Raman scattering has a special multi-peak structured spectrum with the maximum ~13.2 THz away from the pump frequency. Thus, through all the simulations frequency dependency of Raman gain coefficient is approximated by second order parabola profile.

$$\begin{aligned} &In\ frequencydomain: \\ &\alpha_g = \alpha_g \left[1 - \left(\frac{\Delta w}{w_g} \right)^2 \right] \\ &In\ time\ domain: \\ &\alpha_g = \alpha_g \left[1 + \frac{1}{w_g^2} \frac{\partial^2}{\partial t^2} \right] \end{aligned} \tag{2.5}$$

where $\Delta w = [w_p - w_s] - w_g$ is the frequency shift deviation from $w_g = 13.2THz$ at which the gain is maximum. [18]

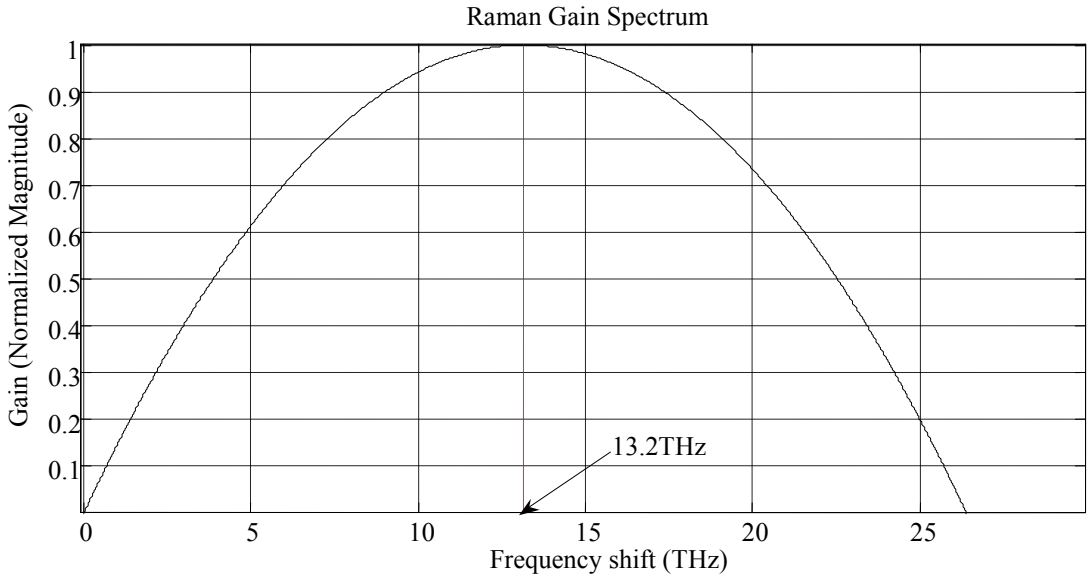

Fig.2.1 Approximated Raman Gain Spectrum.

The band-limiting property of Raman gain spectrum acts as a band-pass filter. For our case the exponential of this spectrum forms a Gaussian band-pass filter with a broad bandwidth.

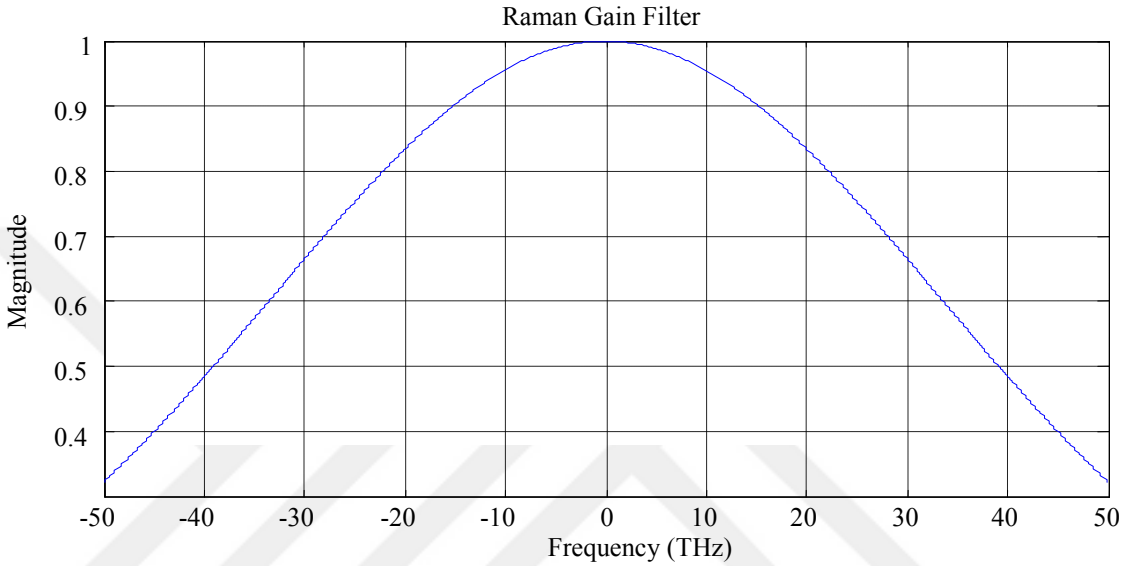

Fig. 2.2 Raman gain filter with Gaussian profile.

After all effects as saturation and frequency dependency are included, the Raman gain is calculated as:

$$\alpha_g(t,z) = \alpha_g^0 \exp\left[-\left(\frac{t-(z/v_{gp}-z/v_{gs})}{\tau_p}\right)^2\right] + \alpha_g^0 \frac{1}{w_g^2}\frac{\partial^2}{\partial t^2}$$

where

$$\alpha_g^0 = \left[\frac{g_R \dfrac{P_p^0}{1+\dfrac{\left|A_s^0\right|^2}{P_{sat}}} l_g}{}\right] \tag{2.6}$$

2.2 Simulation Set up and Parameters

To generate the first order Raman Soliton pulses, two-fiber configuration was used. The set up of the simulation is summarized in the Figure 2.3 below.

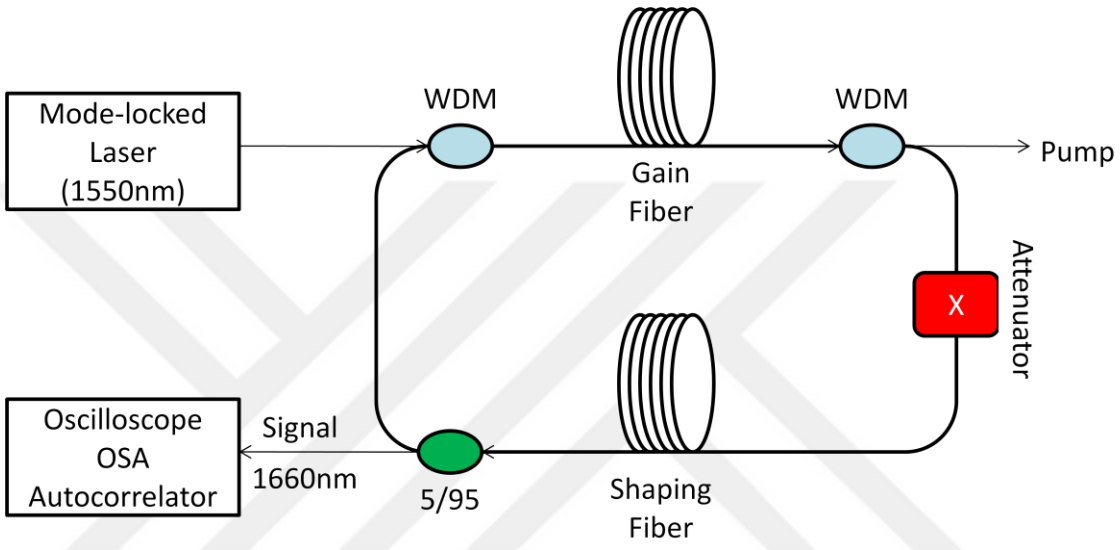

Fig. 2.3 First order Raman Soliton Laser Simulation set up.

In the simulations, 10ps (FWHM) transform-limited Gaussian pulses from Mode-Locked color-center laser operating at 1550nm and having ~ 40nm tunability, was used to generate Raman signal pulses synchronously. Since the Raman frequency shift of ~13.2 THz corresponds nearly to 110nm shift at 1550nm, Raman pulses are generated at around 1660nm and can be tunable due to pump wavelength. The cavity consists of 100m dispersion shifted (Corning Vascade) gain fiber which has -3 (ps/km-nm) dispersion and 0.05 (ps/km-nm2) dispersion slope at 1550nm. The dispersion and the GVD profile of the dispersion shifted fiber used in the simulations can be approximated by a linear equation as:

$$D \cong -3 + 0.05(\Delta\lambda) \qquad where \qquad \Delta\lambda = \lambda - 1550nm$$

$$\beta_2 = -\frac{\lambda^2}{2\pi c} D \tag{2.7}$$

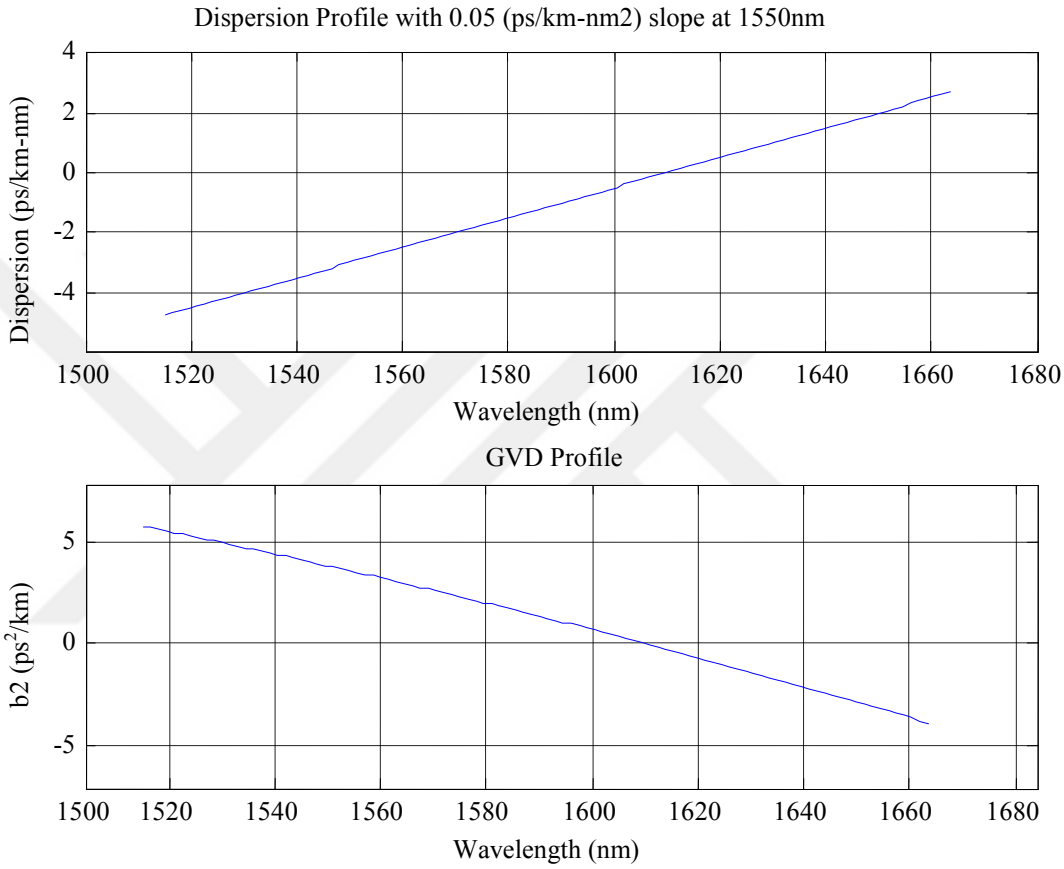

Fig. 2.4 Dispersion and the GVD profile of the DSF.

Due to material dispersion which is the frequency dependency of refractive index, pump and Stokes pulses at different wavelengths travel at different speeds. This causes both pulses slide over each other through the propagation. Walk-off between the pulses ($\Delta t = z/v_{gp} - z/v_{gs}$) can be calculated by using dispersion profile of the fiber. Integral of the dispersion from the pump to the Stokes wavelength gives the corresponding walk-off time per unit length. Thus the total walk-off between the pulses in one round trip is:

$$\Delta t = \left[\int_{\lambda_p}^{\lambda_s} D(\lambda) d\lambda \right] l_g \tag{2.8}$$

The wavelength of the pump signal determines both the output Stokes signal wavelength and corresponding walk-off time. Thus, walk-off between the pulses changes when we tuned the pump wavelength. The walk-off times between the corresponding Stokes and the pump pulses (~110nm down-shifted) are shown in the Figure 2.5 below.

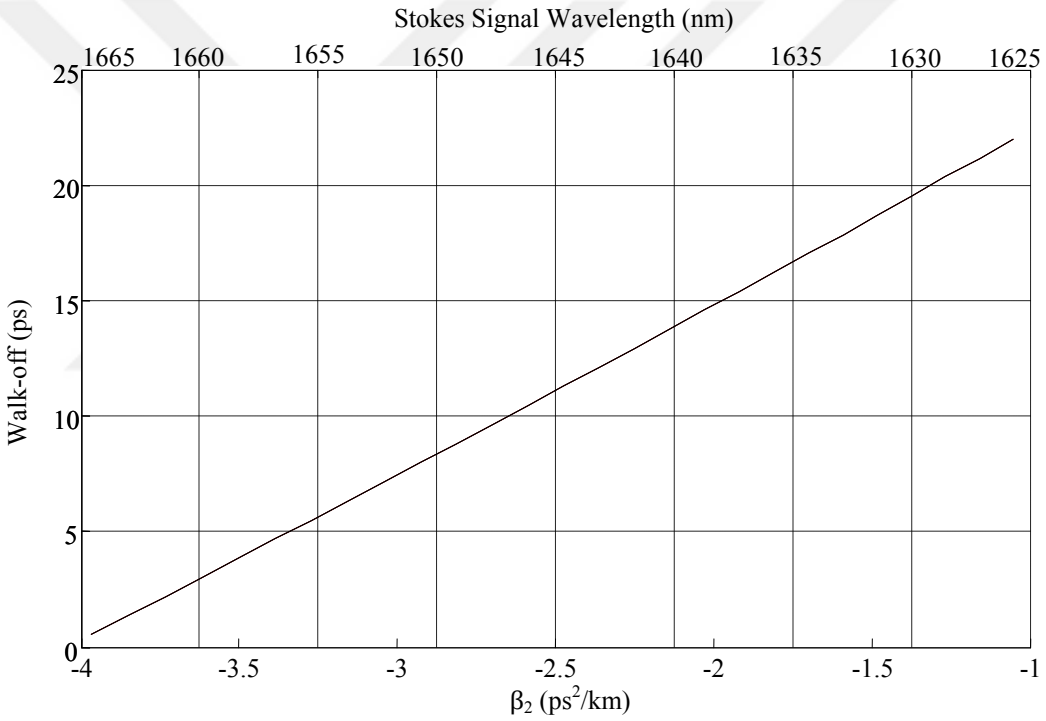

Fig. 2.5 Walk-off time between the Pump and Stokes pulses.

As a result of walk-off between the pulses, the overlapping length decreases and so does the gain. The effect of the walk-off on the gain can be explained as the effective gain length becomes shorter than the actual length.

In simulations, SSFM (Split Step Fourier Method) is used to analyze the propagation of pulses. The parameters used in the simulation are summarized in a table below.

Table 2.1 The parameters used in SSFM simulation for 1st order Raman Soliton Laser.

h	*Step size in SSFM*	$0.5m$
dt	*Time increment*	$10\ fs$
l_g	*Gain Length*	$100m$
l_{sh}	*Shaping Length*	$20m$
α	*Fiber Loss*	$0.2\ (dB/km)$
g_R	*Raman Gain coefficient*	$0.8\ (W^{-1}km^{-1})$
γ	*Nonlinearity coefficient*	$2\ (W^{-1}km^{-1})$
X	*Attenuation factor*	%30
C	*Output coupling*	%5

According to these parameters, N (number of steps in gain fiber at every round trip) becomes 200 and the distributed loss acting on the Stokes pulse by the cavity at each circulation becomes $\alpha_{loss} = \alpha(l_g + l_{sh}) - \ln(0.95X) = 0.4$. In order to focus the gain more on the central part of the Stokes pulse, pump is adjusted in a way that it spans the Stokes pulse from left to right symmetrically by tuning the repetition rate of the Mode-locked laser.

At steady state the gain and loss acting on the Stokes pulse through the beginning to the end of the cavity becomes equal. The peak power of the Stokes pulse P_s^{peak} at steady state can roughly be estimated by the following formula. In this equation Δt_0 is the walk-off at each step size (h) and τ_p is the pump pulse width.

$$\alpha_{gain} \approx g_R P_p^0 h \sum_{n=-N}^{N} \frac{\exp\left[-\left(\frac{n\Delta t_0}{t_p}\right)^2\right]}{\left(1+\frac{P_s^{peak}}{P_{sat}}\right)^{N+n+1}} \approx a_{loss} = 0.4$$

where

$$P_{sat} = \frac{1}{g_R^{"} h} \qquad and \qquad g_R^{"} = \left(\frac{w_p}{w_s}\right) g_R \tag{2.9}$$

2.4 Simulation Results and Discussion

To analyze the performance of the set up, pump pulses ranging from 1515nm to 1554nm with the increment of 1.5nm were used to generate stable, soliton pulses at 1625nm to 1664nm Stokes wavelengths. Since each pump and the Stokes pulse combination has different group-velocity dispersion (GVD) and walk-off behavior, both the required pump and the output signal characteristics are different from each other. To eliminate the walk-off between the pulses, pump wavelength should be selected such that the zero dispersion wavelength of the fiber should be nearly in the middle of the pump and the Stokes signal wavelengths. For our case, the zero dispersion of the fiber is nearly at 1610nm which means the pump signal at 1550nm should be used to eliminate almost all the walk-off.

Since the walk-off changes the effective gain length, different threshold pump powers are required to generate Stokes pulses at different wavelengths. For Stokes pulses with large walk-off, namely at short wavelengths for our case, the effective gain length decreases more and so the threshold power increases. Based on the gain and loss calculation, the threshold power can be calculated by equating loss to the gain in small signal case where there is no saturation.

$$g_R P_p^0 l_{eff} \approx \alpha_{loss} = 0.4$$

$$where$$

$$l_{eff} \approx h \sum_{n=-N}^{N} \exp\left[-\left(\frac{n\Delta t_0}{t_p} \right)^2 \right] \tag{2.10}$$

To analyze the evolution of Stokes pulses at specific wavelength, twelve different pump powers which span 1.1W regime starting from the corresponding threshold power, are used. Since, the Stokes signal starts to break up for high pump powers, the operating point should be close to threshold.

In the following figures, the output Stokes pulses at 1637nm with β_2= -1.9192 (ps^2/km), 1650nm with β_2= -2.9265 (ps^2/km), and 1664nm with β_2= -3.9662 (ps^2/km) are selected as an example to summarize the evolution of first order Raman Stokes pulses. The output Raman soliton pulse, its peak power and the pulse width evolution through the circulation are shown.

Case1: ($\lambda_p = 1527nm, \lambda_{stokes} = 1637nm, \beta_2^{stokes} = -1.919\, ps^2/km$**)**. Pump power is varied from 8.56W to 9.66W. Particular results obtained for power levels at 8.56W, 8.96W and

4.94W are presented below for discussion. The calculated threshold power for this GVD value is 8.38W. Thus, since the power is very close to threshold as seen below, it requires long time to reach steady state.

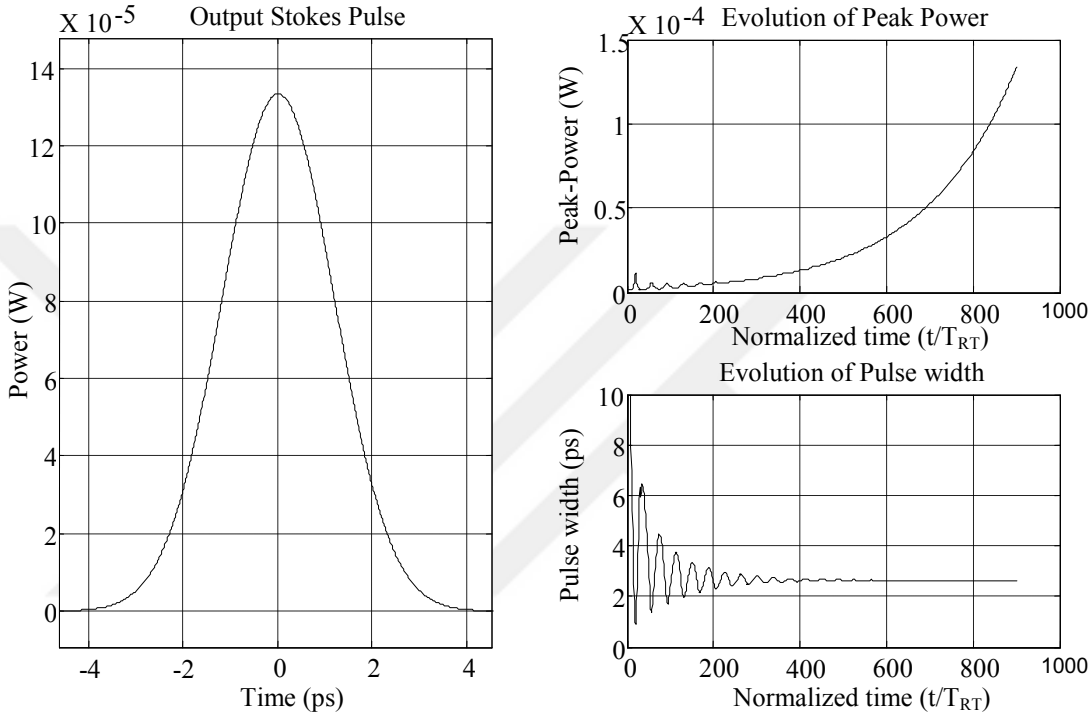

Fig. 2.6 Stokes pulse with β_2=-1.919(ps^2/km) and P_p=8.56 W.

However, when we increase the power to 8.96W, the Stokes pulse reaches steady state that can be understood by looking at the peak-power and pulse width profile through 900 round trips. When we analyze the steady-state output pulse, it perfectly fits to hyperbolic secant square pulse with 1.33ps pulse width and 1.278W peak power.

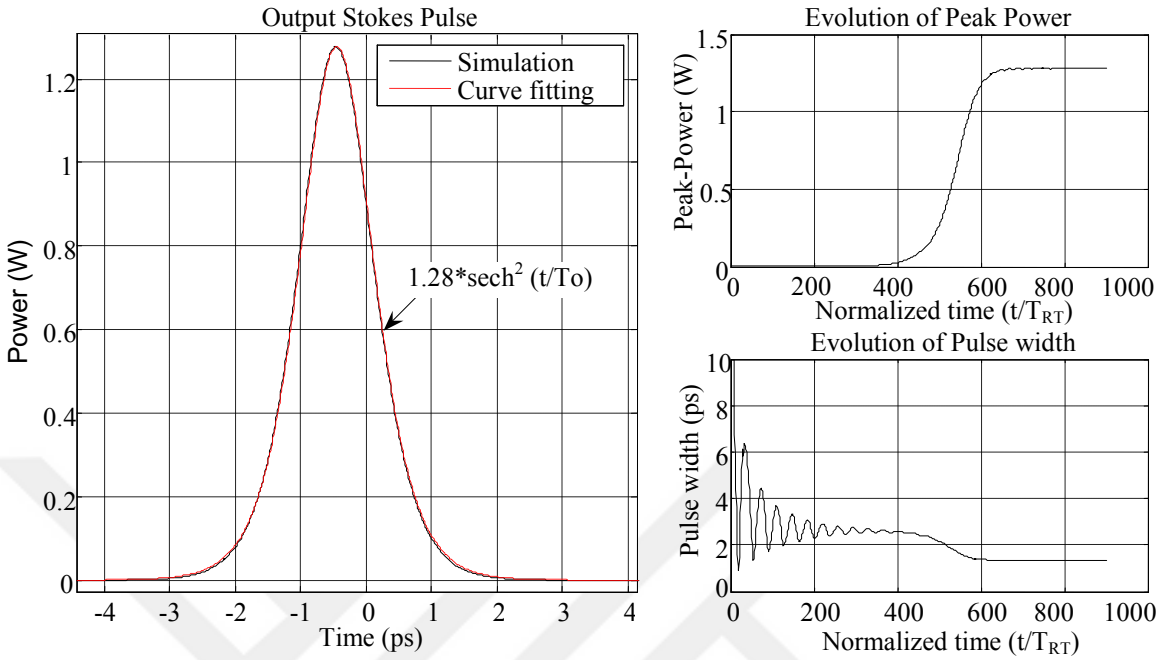

Fig. 2.7 Stokes pulse with β_2=-1.919(ps^2/km) and P_p=8.96 W.

As we increase the pump power more, the pulse starts to break up and release additional energy by extracting dispersive waves as shown in the figure below.

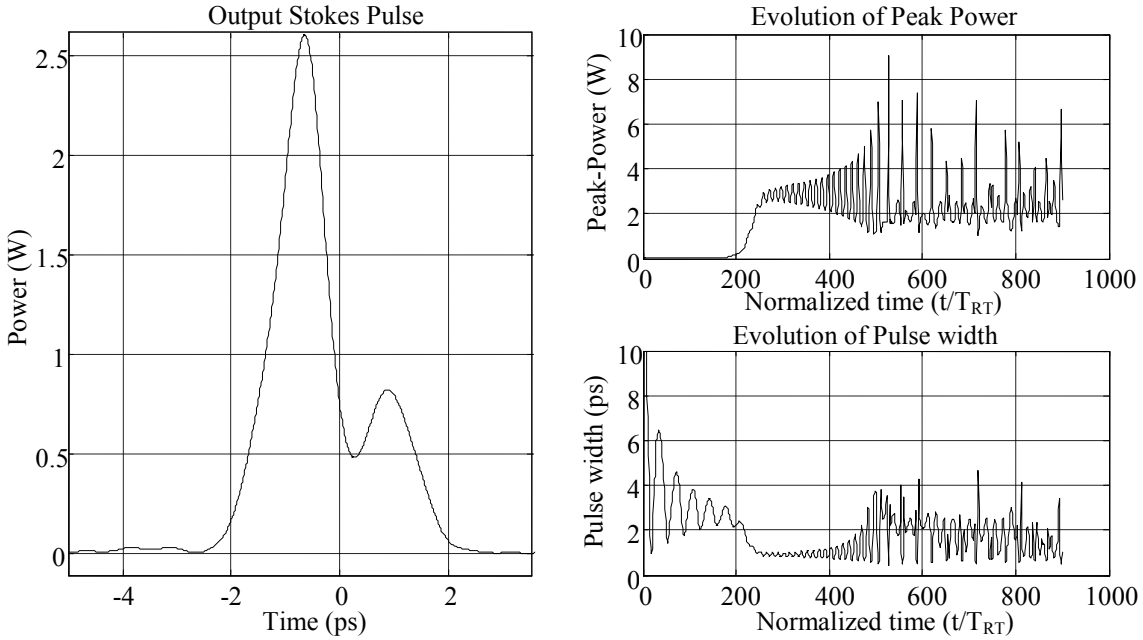

Fig. 2.8 Stokes pulse with β_2=-1.919(ps^2/km) and P_p=9.66 W.

Case2: ($\lambda_p = 1540nm, \lambda_{stokes} = 1650nm, \beta_2^{stokes} = -2.927ps^2/km$). Pump power is varied from 5.98W to 7.08W. Particular results obtained for power levels at 5.98W, 6.38W and 7.08W are presented below for discussion. The calculated threshold power is 5.9W which is less than the previous case because of shorter walk-off. Since the power is very close to threshold as seen below, it reached to steady-state at very low power.

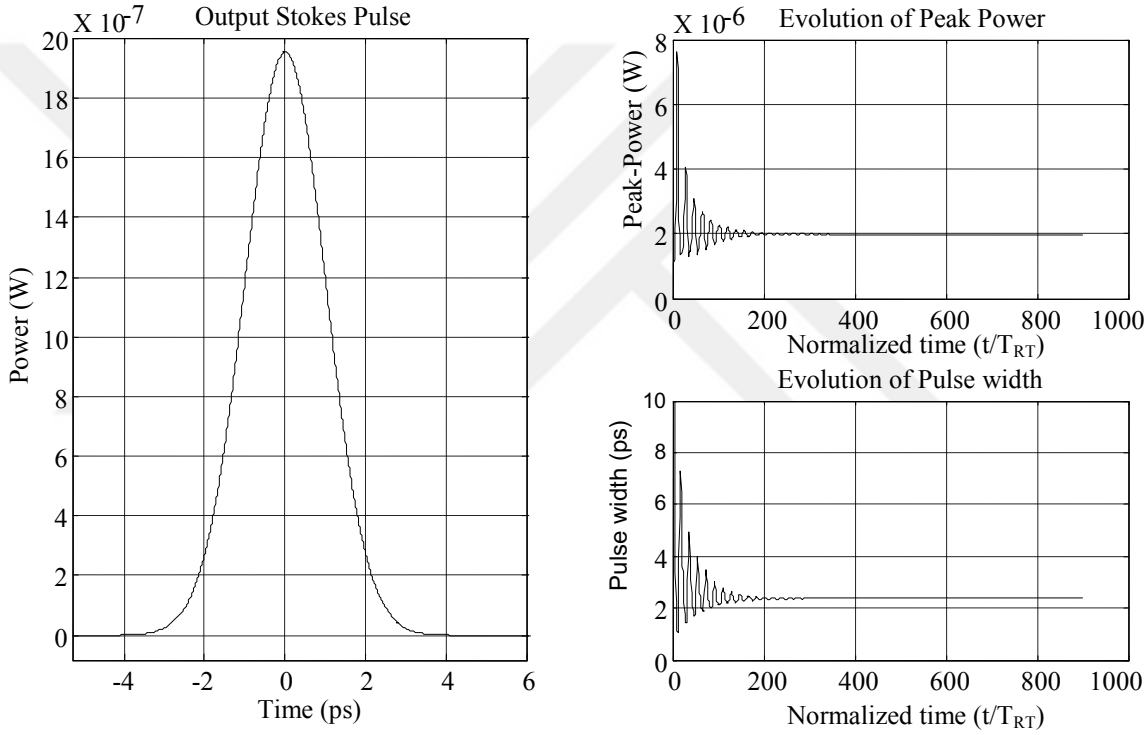

Fig. 2.9 Stokes pulse with β_2=-2.927(ps^2/km) and P_p=5.98 W.

As we increase the power up to 6.38, the Stokes pulse reaches steady state. When we analyze the steady-state output pulse, it perfectly fits to hyperbolic secant square pulse with 1.43ps pulse width and 1.5322W peak power.

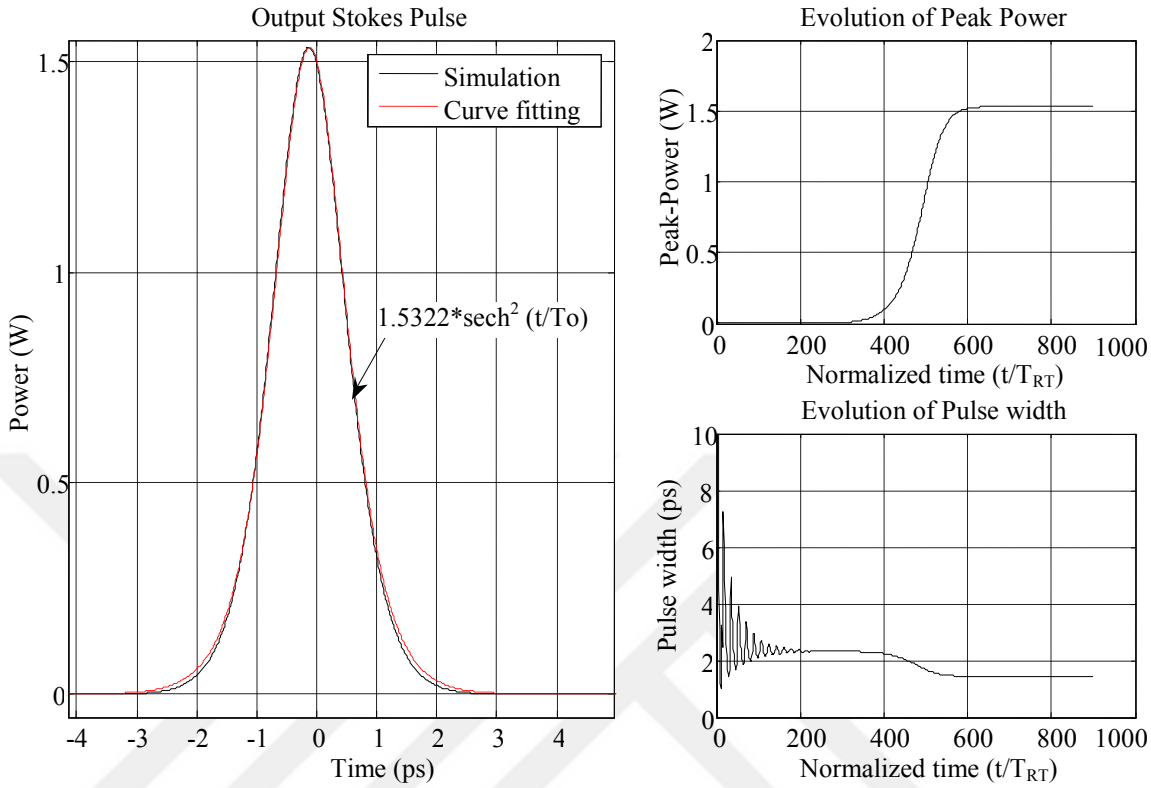

Fig. 2.10 Stokes pulse with β_2=-2.927(ps^2/km) and P_p=6.38 W.

When we increase the pump power more to 7.08W, the pulse starts to break up and release additional energy by extracting dispersive waves as shown in the figure below.

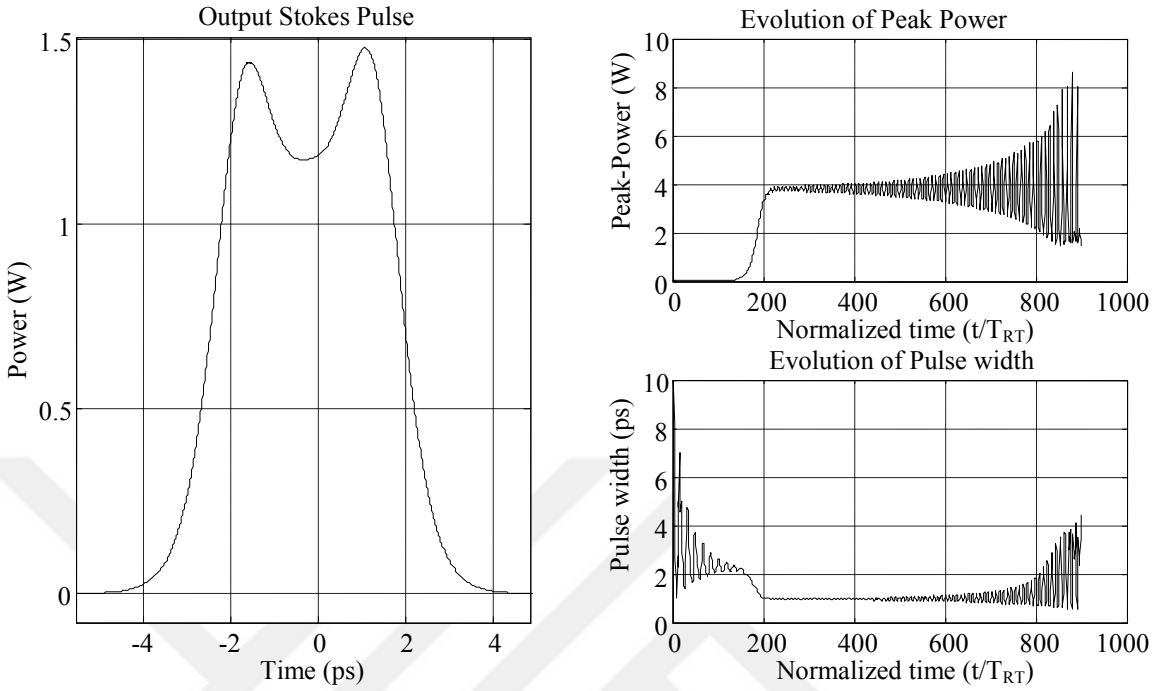

Fig. 2.11 Stokes pulse with β_2=-2.927(ps^2/km) and P_p=7.08 W.

Case3: ($\lambda_p = 1554nm, \lambda_{stokes} = 1664nm, \beta_2^{stokes} = -3.9662\, ps^2 / km$ **)**. Pump power is varied from 5.12W to 6.12W. Particular results obtained for power levels at 5.12W, 5.52W and 6.12W are presented below for discussion.. The calculated threshold power is 5.05W which is less than the previous cases because of much shorter walk-off. Since the pump power is less than the threshold power, pulse cannot build up in the system and attenuates.

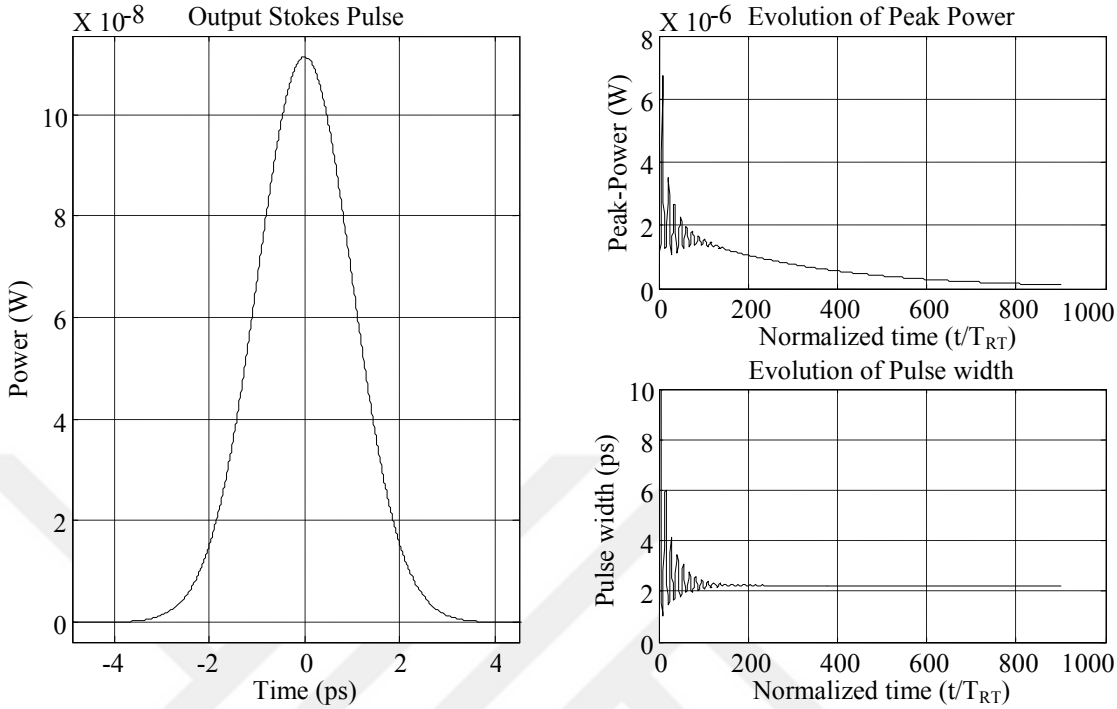

Fig. 2.12 Stokes pulse with β_2=-3.9662(ps^2/km) and P_p=5.12W.

When we increase the power up to 5.52W and 6.12W shown in the following figures, the Stokes pulse reaches the steady state. When we analyze the steady-state output pulse at P_p=5.52 W, it perfectly fits to hyperbolic secant square pulse with 1.34ps pulse width and 1.632W peak power. On the other hand, the output pulse at P_p=6.12 W converges to hyperbolic secant square pulse with 1.09ps pulse width and 3.926W peak power.

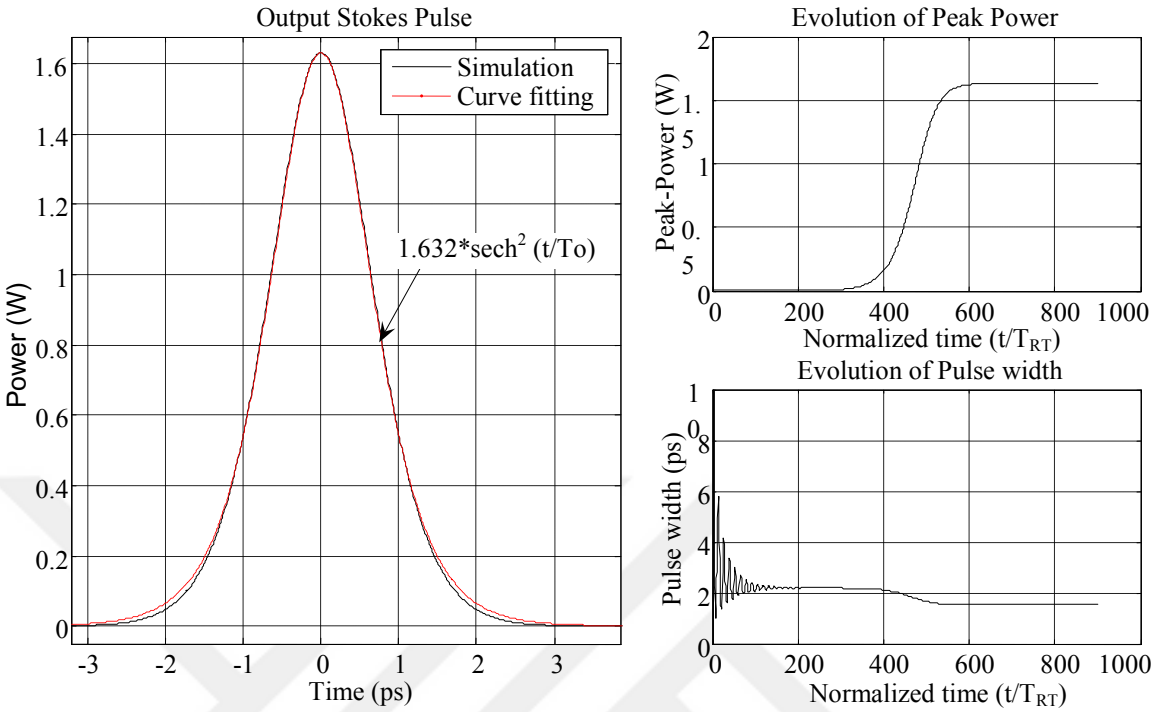

Fig. 2.13 Stokes pulse with β_2=-3.9662(ps^2/km) and P_p=5.52 W.

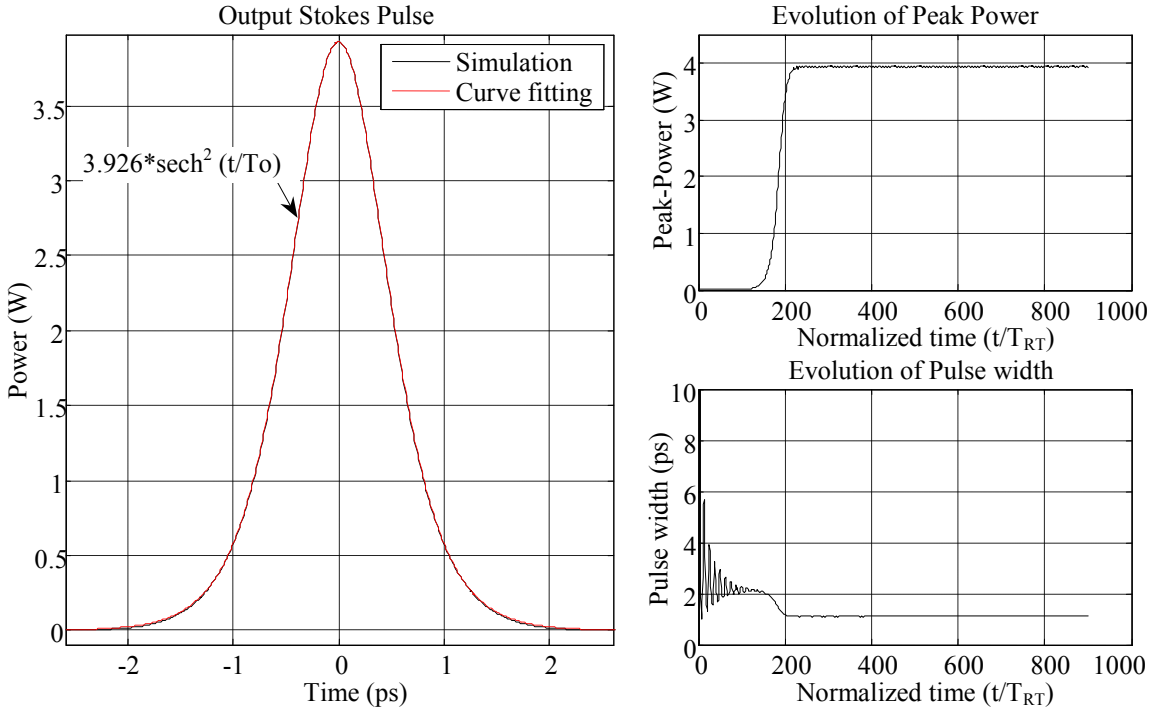

Fig. 2.14 Stokes pulse with β_2=-3.9662(ps^2/km) and P_p=6.12 W.

2.5 The Stability Analyses

To analyze the stability regime of the generated Stokes signals where they converge to a hyperbolic secant square soliton pulse, SSFM simulation was repeated at combinations of 27 different Stokes wavelengths and 12 pump powers. The output signals obtained from each simulation was analyzed and categorized as below threshold, saturated or broke up. The results are shown in the following contour plots to investigate the output Stokes signals with respect to their both peak-powers and the pulse widths.

Since the walk-off between the pump and the Stokes pulses is highly dependent to the GVD parameter, the threshold required to generate the Stokes signal is different at each wavelength. As a result, the pump power for each GVD value (namely for each Stokes wavelength) is varied in a 1.1W regime starting from the corresponding threshold which is estimated by using equation 2.10. In the following contour plots, the pump power index is used instead of the actual power for each GVD value. The actual pump powers applied in the simulations can be calculated by the using the following formula and the estimated threshold powers (P_{th}) shown in the Table 2.2 as:

$$P_p^k(\beta_2) = P_{th}(\beta_2) + k * \Delta p \qquad where \qquad \Delta p = 0.1W \;\; and \;\; k = 1-12(indexnumber)$$

Table 2.2 Calculated Threshold powers at specific GVD values at Stokes wavelength.

Stokes GVD (ps^2/km)	Estimated Threshold Power(W)	Stokes GVD (ps^2/km)	Estimated Threshold Power(W)	Stokes GVD (ps^2/km)	Estimated Threshold Power(W)
-1.0507	11.3	-2.0296	7.77	-3.0405	5.98
-1.1579	11.3	-2.1403	7.77	-3.1548	5.6
-1.2655	10.34	-2.2514	7.07	-3.2695	5.6

-1.3734	10.34	-2.363	7.07	-3.3846	5.33
-1.4818	9.42	-2.4749	7.07	-3.5001	5.33
-1.5906	9.42	-2.5872	6.47	-3.616	5.33
-1.6997	9.42	-2.6999	6.47	-3.7323	5.17
-1.8093	8.56	-2.813	5.98	-3.849	5.17
-1.9192	8.56	-2.9265	5.98	-3.9662	5.12

Figure 2.15 shows the peak powers of the converging Stokes pulses at specific GVD walk-off and pump power. Also, the region (upper-left) where the pulses break up is highlighted in the graph.

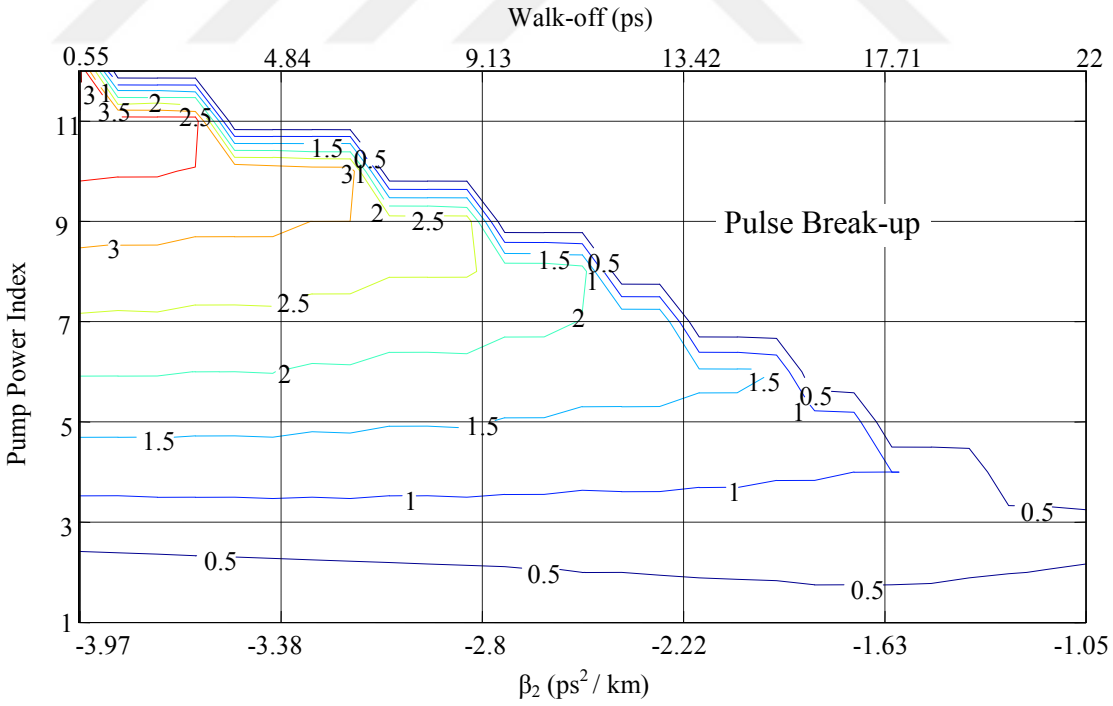

Fig. 2.15 Stability region contour plot with respect to Stokes peak power.

As seen in the figure, laser does not reach the threshold and pulse cannot build up in the system for low pump powers (below or in a very close vicinity of threshold) independent of operating wavelength. With increase in the pump power, Stokes pulses starts to be generated and reach to steady state. The width of stability regime for each GVD value, however, is directly proportional to GVD at Stokes wavelength and the walk-off between the pump and Stokes pulses. Since the Stokes signal power is much less than the pump and the XPM is as twice as effective than the SPM, walk-off becomes very important to control the effectiveness of pump induced XPM on the Stokes signal. Pump signal with 10ps pulse width is quite wide compared to the Stokes pulse with nearly 1ps pulse width. If the walk-off is small, the Stokes pulse experiences only the central part of the pump signal. Thus, the pump induced XPM on the Stokes signal becomes almost linear, which has no drastic effect on the spectrum rather than shift in frequency domain. However, if the walk-off is large, pump induced XPM on the Stokes signal drastically distorts the spectrum. As a result, even for small GVD values Stokes pulse cannot maintain its shape and breaks up. In addition to walk-off, GVD value determines the limit up to which peak power the nonlinearity can be tolerated. The positive chirp due to XPM and SPM must be balanced by the negative chirp due to GVD. The less the group velocity dispersion is, the less the nonlinearity can be tolerated.

In the following analysis, stability region is investigated with respect to final pulse width. As illustrated in Figure 2.16, the final pulse width the Stokes signals converges to is highly dependent on the pump power and the dispersion values. Also, the regions where the pulse cannot build up and break up due to excessive nonlinearity are highlighted in the graph.

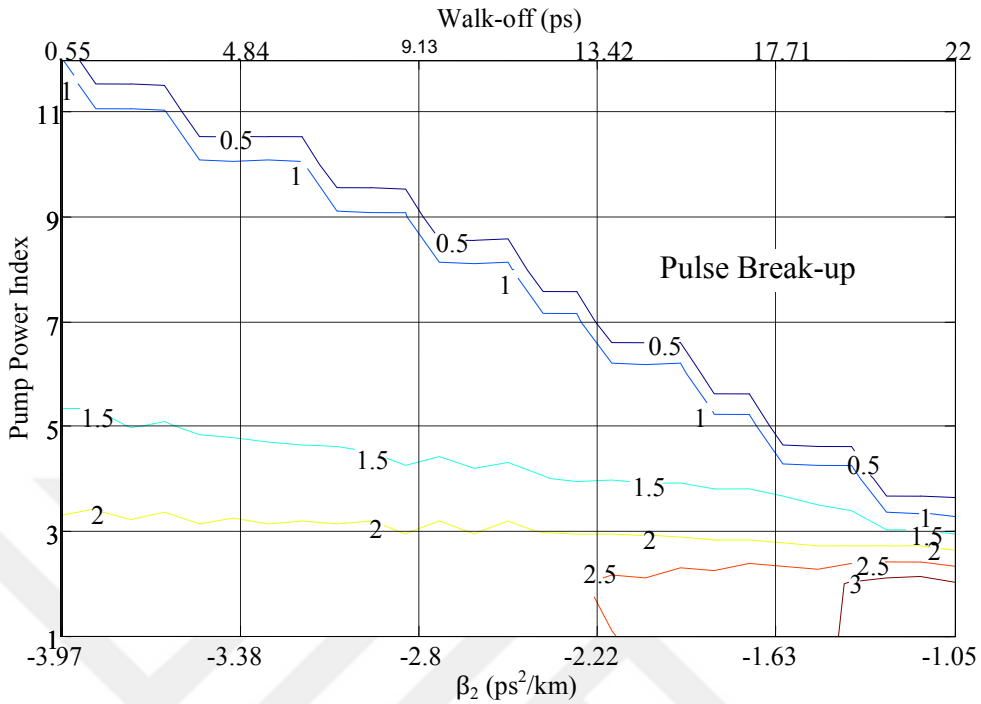

Fig. 2.16 Stability region contour plot with respect to Stokes pulse width.

Since SSFM is not efficient computationally, pulse evolution for each Stokes wavelength and the pump power combination is iterated only by N=900 round trips. Thus, for some cases especially for low pump powers (close to threshold), the number of round trips is not enough to enable the generated Stokes pulses to reach steady state. The ambiguity in the bottom left region of the Figure 2.16 represents the unsaturated Stokes pulses with much wider pulse widths than the ones at steady state.

The pulse width of the output Stokes signal shown in the previous figures converges to its final value that almost satisfies the fundamental soliton condition as $N^2 = \frac{L_D}{L_{NL}} = \frac{\gamma P_0 T_0^2}{|\beta_2|} = 1$. Thus, both the GVD value at that wavelength and the peak power of the signal determine the output pulse width. It is shown in the following figures

(three different cases as an example) to which soliton order the output Stokes pulses converge. Since the set up consists of an attenuator and a coupler, the pulse suddenly decreases in intensity. Thus, at these points the soliton pulses have different soliton orders.

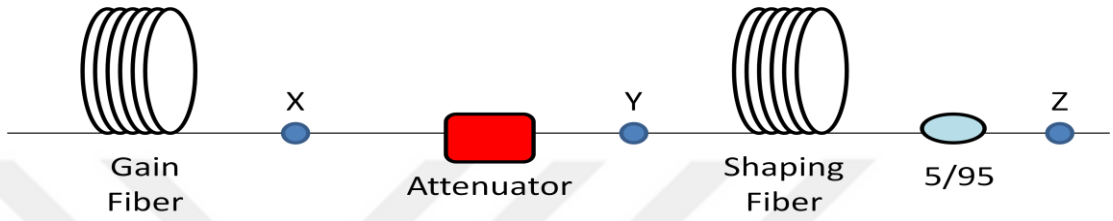

Fig. 2.17 X, Y and Z are three different positions in the cavity where the Stokes pulses analyzed.

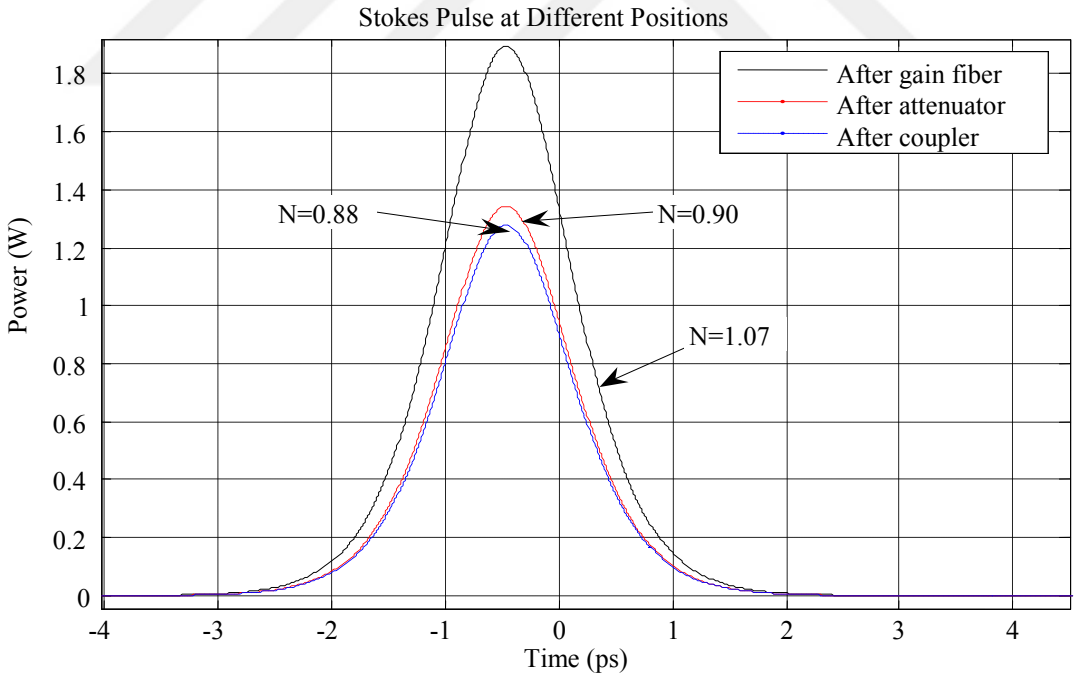

Fig. 2.18 Stokes pulses ($\lambda = 1637nm$, $\beta_2 = -1.9192(ps^2/km)$ *and* $P_p = 8.96W$) at points X, Y and Z with converged soliton order N.

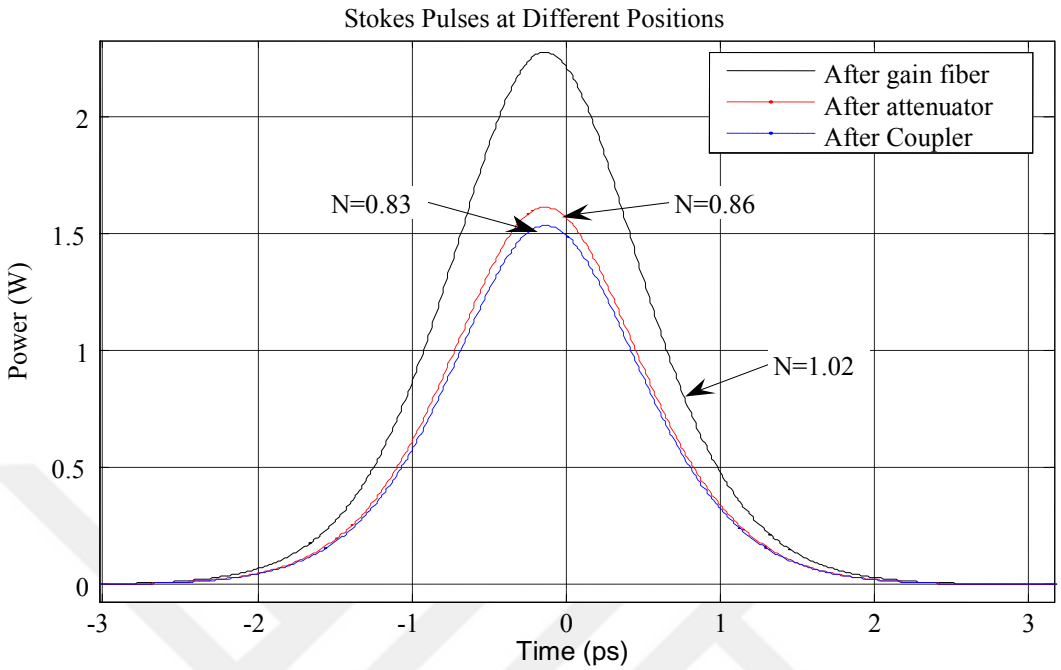

Fig. 2.19 Stokes pulses ($\lambda = 1650nm,\ \beta_2 = -2.9265(ps^2/km)\ and\ P_p = 6.38W$) at points X, Y and Z with converged soliton order N.

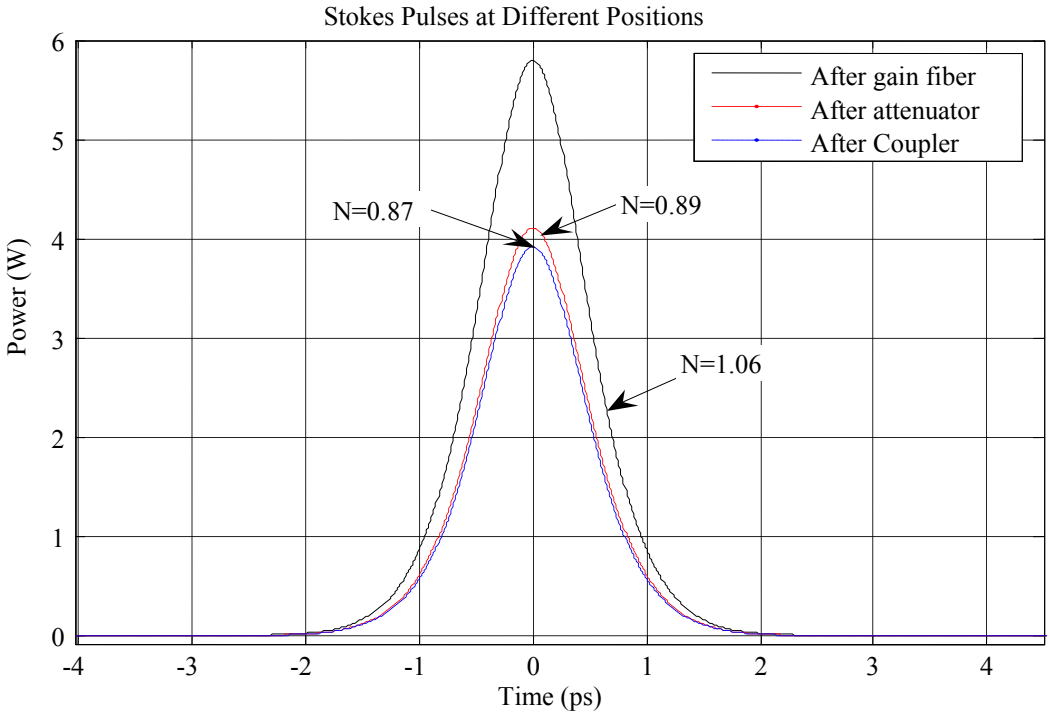

Fig. 2.20 Stokes pulses ($\lambda = 1664nm,\ \beta_2 = -3.9662(ps^2/km)\ and\ P_p = 6.12W$) at points X, Y and Z with converged soliton order N.

CHAPTER 3

SECOND ORDER RAMAN SOLITON LASERS AND STABILITY ANALYSIS

Fiber Raman Soliton Laser is generally designed to generate first order Raman Stokes signal. However, the Raman laser output at first order Stokes wavelength can act as a pump for the cascaded generation of higher order Raman lasing at much longer wavelengths. Cascaded Raman lasing enables to generate coherent laser pulses at very broad range where it is difficult to achieve by other methods [20]. Since the fiber is the gain medium for cascaded lasing of high-order Raman Stokes signals, the Stokes signals at higher orders may also converge to a soliton at steady state.

To assess the conditions where second order solitons can be generated we developed a numerical and analytical formula that includes the nonlinear and linear effects of fibers and interactions between pump lasers and Stokes signals at the first and the second order. The mutual interaction between the pump pulse, first and the second-order Stokes pulses is governed by a set of three non-linear Schrodinger equations including all processes of GVD, SPM, XPM, walk off between the pulses, Raman gain and pump depletion as: [5]

$$\frac{\partial A_p}{\partial z}+\frac{1}{v_{gp}}\frac{\partial A_p}{\partial t}+i\frac{\beta_{2p}}{2}\frac{\partial^2 A_p}{\partial t^2}+\frac{\alpha_p}{2}A_p=i\gamma_p(\left|A_p\right|^2+2\left|A_{s1}\right|^2+2\left|A_{s2}\right|^2)A_p+R_p(z,t)$$

$$\frac{\partial A_{s1}}{\partial z}+\frac{1}{v_{gs1}}\frac{\partial A_{s1}}{\partial t}+i\frac{\beta_{2s1}}{2}\frac{\partial^2 A_{s1}}{\partial t^2}+\frac{\alpha_{s1}}{2}A_{s1}=i\gamma_{s1}(\left|A_{s1}\right|^2+2\left|A_{s2}\right|^2+2\left|A_p\right|^2)A_{s1}+R_{s1}(z,t) \quad (3.1)$$

$$\frac{\partial A_{s2}}{\partial z}+\frac{1}{v_{gs2}}\frac{\partial A_{s2}}{\partial t}+i\frac{\beta_{2s2}}{2}\frac{\partial^2 A_{s2}}{\partial t^2}+\frac{\alpha_{s2}}{2}A_{s2}=i\gamma_{s2}(\left|A_{s2}\right|^2+2\left|A_{S1}\right|^2+2\left|A_p\right|^2)A_{s2}+R_{s2}(z,t)$$

where $v_{gp,gs1,gs2}$ is the group velocity, $\gamma_{p,s1,s2}$ is the nonlinearity coefficient, $\beta_{2p,2s1,2s2}$ is the GVD parameter and $A_{p,s1,s2}$ is the amplitude of the pump, first order Stokes and the second order Stokes signals respectively. R_p is the pump depletion and $R_{s1,s2}$ is the Raman gain coefficient for the Stokes signals.

In a cascaded Raman laser system, nth order Stokes signal is generated by (n-1)th order Stokes and acts as a pump for (n+1)th order Stokes signal. For our case, we only aim to generate first and second order Raman Stokes signals.

In order to generate the first order Stokes pulse, pump power must be greater than the threshold of the first order. When the threshold power condition is met, first order Stokes pulse starts to build up in the cavity through the circulation. On the hand, second order Stokes signal cannot be generated until the first order Stokes signal has enough energy to build up a gain that compensates the loss of the second order. Once the second order Stokes is generated, the generated second order Stokes pulses acts as a new loss mechanism for the first order Stokes and thus decreases the slope efficiency.

First and the second order Stokes pulses propagate in two different cavities where they only interact through the gain fiber. Thus, the threshold powers required to generate first and the second order Stokes are not the same. They are determined by each cavity. Fiber losses, attenuation factor and the output coupling in each cavity define its threshold power.

3.1 Time-Dependent Gain and the Loss on the Propagating Pulses

As discussed in the previous chapter, first order Stokes pulse experiences a time dependent gain through the propagation in a cavity and reaches steady state when the gain becomes equal to the loss. There is no other loss acting on the first-order Stokes pulse rather than fiber loss, attenuation and coupling losses. However, in this case the generation of second order Raman Stokes is reflected as an additional loss for the first-order pulses. On the other hand, second order Stokes pulse only experiences a gain induced by first order Stokes. The effective gain and the loss on the pulses through the gain-fiber (treated as step by step with the step size h) are summarized below.

1) Pump signal is the main source of energy to generate all the Stokes signals. There is no gain on the pump signal, it attenuates due to fiber loss as $P_p \exp(-\alpha l_g)$ and transfers energy to generate first-order Stokes pulse. The depletion of the pump signal due to first order Raman Stokes is as follows:

$$P_p = P_p \exp\left(-g_{R1}^{''}\left|A_{s1}^0\right|^2 l_g\right) \approx P_p \frac{1}{1+\frac{\left|A_{s1}^0\right|^2}{P_{sat1}}}$$

$$P_{sat1} = \frac{1}{g_{R1}^{''} l_g} \quad and \quad g_R^{''} = \left(\frac{w_p}{w_{s1}}\right) g_{R1} \quad and \quad \left|A_{s1}^0\right|^2 = Peak\ signal\ power \tag{3.2}$$

where g_{R1} and $g_{R1}^{''}$ are the Raman gain coefficient for the first order Stokes and depletion coefficient for the pump signals, respectively.

2) First-order Stokes signal is amplified by the pump signal. The time dependent gain in which frequency dependency, walk-off and the saturation effects are included, is:

$$\alpha_{g1}(t,z) = \alpha_{g1}^0 \exp\left[-\left(\frac{t-(z/v_{gp}-z/v_{gs1})}{\tau_p}\right)^2\right] + \alpha_{g1}^0 \frac{1}{w_g^2}\frac{\partial^2}{\partial t^2}$$

$$where \tag{3.3}$$

$$\alpha_{g1}^0 = \left[\frac{g_{R1}\frac{P_p^0}{1+\frac{\left|A_{s1}^0\right|^2}{P_{sat}}} l_g}{}\right] \quad and \quad P_{sat} = \frac{1}{g_{R1}^{''} l_g}$$

According to the simulation set up, total distributed loss in which attenuation and coupling factors are treated as distributed loss is calculated as $\alpha_{loss} = \alpha l_g - \ln(CX)$ where α is the fiber loss coefficient, l_g is the length of the gain fiber, C is the coupling percentage and X is the attenuation factor. In addition to cavity loss, first order Stokes signal transfers energy to generate second order Stokes pulses. Thus, the evolution of the second order Stokes signal depletes the first order Stokes as:

$$|A_{s1}|^2 = |A_{s1}|^2 \exp\left(-g_{R2}^{"}\left|A_{s2}^0\right|^2 l_g\right) \approx |A_{s1}|^2 \frac{1}{1+\frac{\left|A_{s2}^0\right|^2}{P_{sat}^{'}}}$$

$$P_{sat1}^{"} = \frac{1}{g_{R2}^{"} l_g} \quad and \quad g_{R2}^{"} = \left(\frac{w_{s1}}{w_{s2}}\right) g_{R2} \quad and \quad \left|A_{s2}^0\right|^2 = Peak\,signal\,power$$

where g_{R2} and $g_{R2}^{"}$ are the Raman gain coefficient for the second order Stokes and depletion coefficient for the first order Stokes signals, respectively.

3) Second order Stokes signal is generated and amplified by the first order Stokes signal by stimulated Raman scattering. The effective gain on the pulse becomes: [18]

$$\alpha_{g2}(t,z) = \alpha_{g2}^0 \exp\left[-\left(\frac{t-(z/v_{gs1}-z/v_{gs2})}{\tau_{s1}}\right)^2\right] + \alpha_{g2}^0 \frac{1}{w_g^2}\frac{\partial^2}{\partial t^2}$$

$$where \qquad (3.4)$$

$$\alpha_{g2}^0 = \left[g_{R2}\frac{\left|A_{s1}^0\right|^2}{1+\frac{\left|A_{s2}^0\right|^2}{P_{sat}}} l_g\right] \quad and \quad P_{sat} = \frac{1}{g_{R2}^{"} l_g}$$

Second order Stokes signal attenuates only due to fiber loss and the output coupling. The effective distributed loss acting on the second order Stokes pulses becomes $\alpha_{loss} = \alpha l_g - \ln(C)$ where α is the fiber loss coefficient, l_g is the length of the gain fiber, and C is the output coupling percentage.

At steady state, all the Stokes pulses converge to their final peak power and pulse width which do not change significantly through one round trip. Thus, the peak power of

the Stokes pulses P_s^{peak} at steady state can roughly be estimated by the equaling the loss and gain acting on themselves.

3.2 Simulation Set up and Parameters

To verify the analytical expectations, set of numerical simulations are performed in a ring cavity illustrated in Figure 3.1. Ring cavity with the corresponding couplers functions as a partially reflective mirror placed at the ends of the gain fiber and enables the pulses to resonate. Wavelength division multiplexers (WDM) are used at the connections to combine and separate the pulses at different wavelengths. Cavity for the 1st order Stokes signal also includes an attenuator which represents all the bulk losses inside cavity and functions as a balance mechanism to prevent the generated Stokes pulses to break up due to excessive power dependent nonlinear effects.

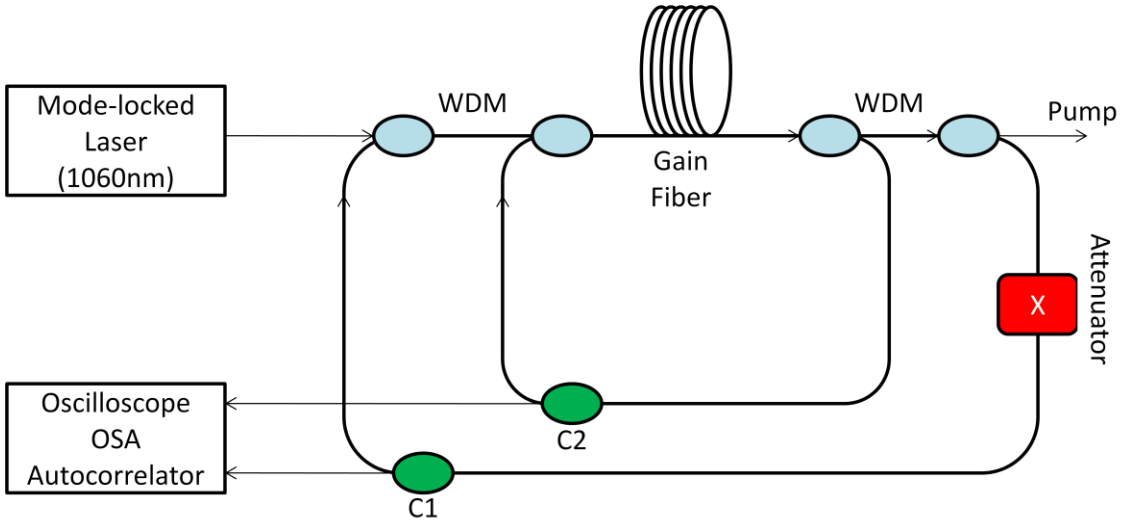

Fig. 3.1 Second order Raman Soliton laser Simulation Set up.

In the simulations, transform-limited Gaussian pulses with 10ps (FWHM) pulse width and 3W to 5W peak power, were used as a pump signal. For the pump signal,

$(\lambda_p = 1060nm \ \ and \ \ \beta_2 \approx -0.23 ps^2/km)$ the dispersion length $L_D = \frac{T_0^2}{|\beta_2|}$ becomes more than 140km and nonlinear length $L_{NL} = \frac{1}{P_0 \gamma}$ becomes around 100m ($\gamma = 3W^{-1}km^{-1}$). Since the condition $L_D >> l_g > L_{NL}$ is satisfied, GVD effect on the pump pulse in equation (3.1) can be neglected and the pump pulse propagation can be treated as in a SPM dominated regime. Because the peak powers of the first and second order Stokes signals are much less than pump power, XPM effect can also be neglected. Thus, it propagates without changing its shape in time domain except being attenuated due to fiber loss and depletion. However, for the Stokes signals both dispersive and nonlinear effects are strongly effective. Both first and the second order Stokes pulses evolve from a pre-defined low DC background through stimulated Raman amplification.

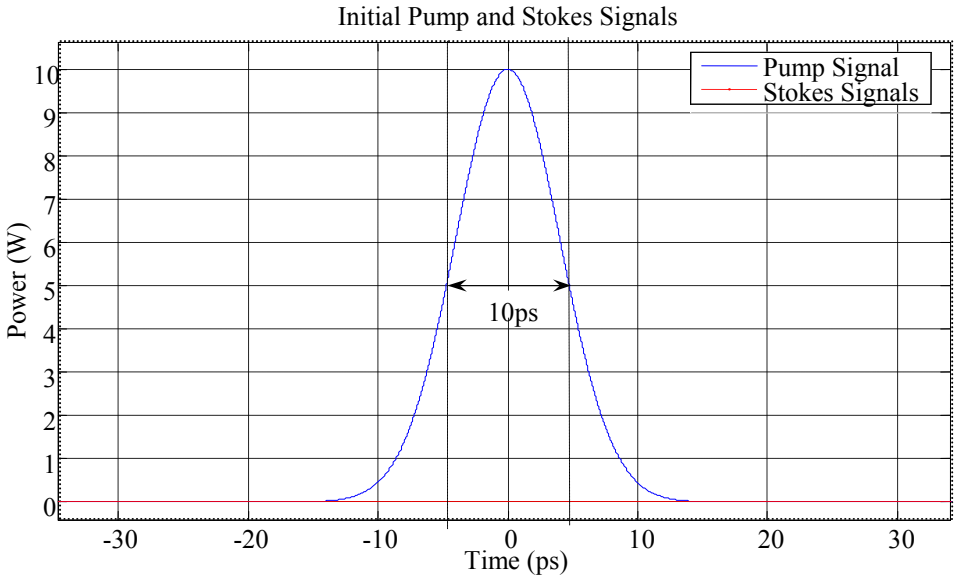

Fig. 3.2 Initial pump, first and the second order Stokes pulses.

Each Stokes pulse as shown in the set up propagates in a different cavity where they only interact through the common gain fiber. Gain fiber is the key component of the

set up and should be selected carefully to minimize the walk-off between the pulses. For the first order Raman soliton laser analyzed in chapter 2, the walk-off can be eliminated by using a commercial DSF with zero dispersion in the middle of the pump and Stokes signal wavelengths. However, for the second order Raman soliton laser, since three pulses with large frequency separation, propagate inside the fiber it is impossible to eliminate walk-off between all the pulses completely. Thus, to minimize the walk-off between the pulses, fiber with low dispersion value over a broad range, i.e. dispersion flattened fiber, should be used. When we searched such fibers in literature, it points out the photonic crystal fibers. Photonic crystal fibers can be designed with a flattened near zero dispersion profile. The gain fiber used in our set up is a special photonic crystal fiber which has a flattened near zero dispersion profile (DFF-PC) in a very broad range. The fabricated photonic crystal fiber and measurement results of its dispersion profile are shown in the following figures.

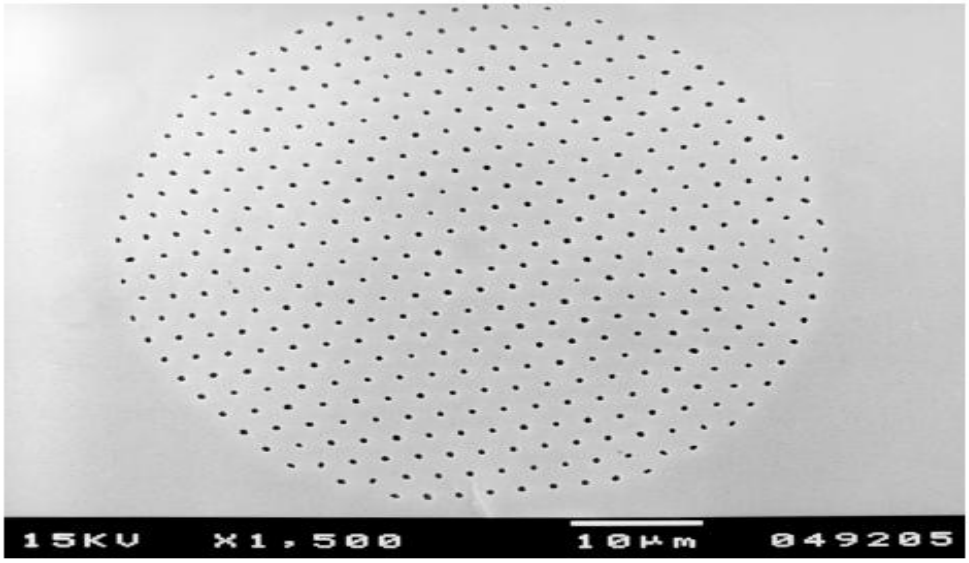

Fig. 3.3 Ultra-flattened dispersion photonic crystal fiber with 11 periods. $\Lambda = 2.47\mu m$ and an average d of $0.57\mu m$. [19]

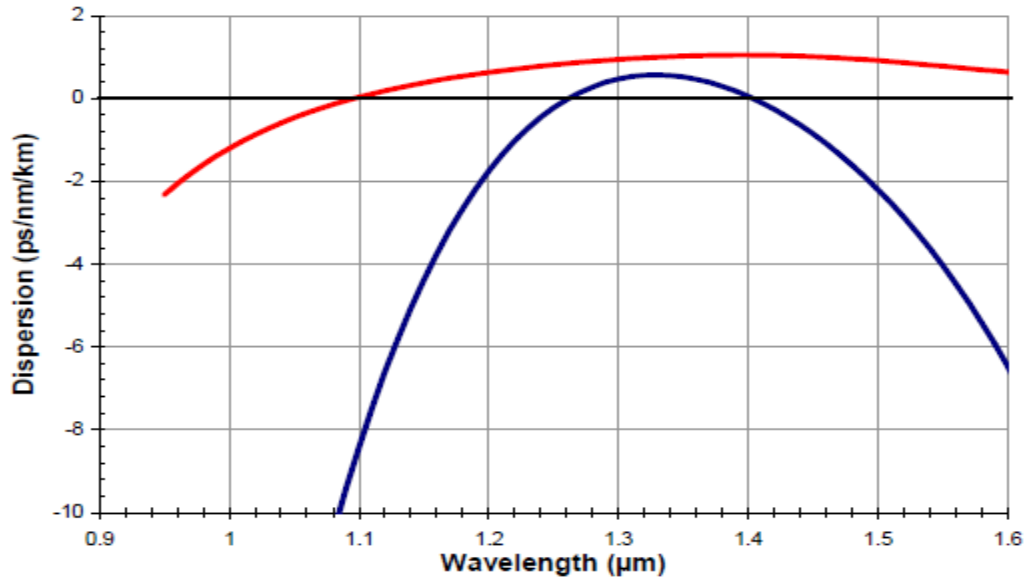

Fig. 3.4 Measured dispersion plots for ultra flattened dispersion PCF similar to the fiber shown in Figure 3.3. Red (upper) curve: d = 0.58, Λ = 2.59, dark (below) blue curve: d= 0.57, Λ=2.47. [19]

This photonic crystal fiber, as shown in the Figure 3.3, has a solid silica core and radially distributed air holes as cladding. There are 11 period of holes between the core and the external jacket. The number of holes can be increased by adding extra ring of holes. By changing the hole diameter (d) and hole-to-hole spacing (Λ), much greater flexibility can be achieved on dispersion profile to satisfy the requirements of an application. [19] As seen in the Figure 3.4, dispersion (red curve) is very close to zero over the wavelength range from 1um to 1.6um. Since the fiber has near zero dispersion profile over broad wavelength range, it is very useful to eliminate the walk-off between the pulses especially between first and the second Stokes pulses with very narrow pulse widths.

According to dispersion profile of this photonic crystal fiber (PCF), it is more reasonable to operate around 1060nm region where the walk-off can be made minimum.

On the other hand, when compared with the DSF (Corning Vascade) with $50um^2$ effective area and zero-dispersion at 1550nm, PC fiber has a $44um^2$ effective area and is operated at 1060nm. Thus, due to both operating wavelength and the composition of the PC fiber, Raman gain and nonlinearity coefficients are scaled by ~1.5. In addition, due to air holes, the confinement loss of the photonic crystal fiber is quite higher than DSF (more than 0.4dB/km).

Table 3.1 The parameters used in SSFM simulation for 2nd order Raman Soliton laser.

h	*Step size in SSFM*	$1m$
dt	*Time increment*	$10\,fs$
l_g	*Gain Length*	$100m$
α	*Fiber Loss*	$0.4\ (dB/km)$
g_R	*Raman Gain coefficient*	$1.2\ (W^{-1}km^{-1})$
γ	*Nonlinearity coefficient*	$3\ (W^{-1}km^{-1})$
X	*Attenuation factor*	%30
$C1$	*Output coupling for* 1^{st} *Stokes*	%5
$C2$	*Output coupling for* 2^{nd} *Stokes*	%0.2
N	*Number of round trips*	4000

3.3 Simulation Results and Discussion

To generate first and the second order Raman soliton pulses simultaneously, the proper pumping condition should be selected. To analyze the performance of the set up, the

pump is tuned to operate at five different wavelengths as 1060nm, 1080nm, 1100nm, 1120nm and 1140nm. The first and the second order Stokes signals are generated at $\Delta v = 13.2 THz$ downshifted frequency which corresponds to $\Delta\lambda \approx 52 nm$ for the first order and $\Delta\lambda \approx 110 nm$ for the second order. Since the optical solitons occur only in an anomalous ($\beta_2 < 0$) dispersion regime, the wavelength of the pump signal cannot be tuned below 1060nm. Thus, the walk-off between the 1st and the 2nd order Stokes signals cannot be eliminated completely. In order to minimize the walk-off between the Stokes pulses, the pump wavelength should be tuned to 1060nm which generates 1st order Stokes at ~1100nm where the dispersion is almost zero. Compared to Stokes pulses with sub-picosecond pulse widths, the pump signal with 10ps pulse width is broad enough to compensate the walk-off to some extent. Thus, the walk-off between the Stokes pulses is more important than the walk-off between the pump and the first order Stokes signals. As a result, according to the dispersion profile of the photonic crystal fiber in Figure 3.4, the optimum condition with respect to walk-off is to use pump signals at ~1060nm. However, there is a trade-off between the walk-off and the robustness to nonlinear effects. If the GVD is very low, the capability of the pulse to compensate the nonlinearity due to SPM and XPM decreases and the Stokes pulses start to break up immediately. Each pump and the Stokes pulse combination, corresponding GVD values and the walk-off between them are shown in Table 3.2.

Table 3.2 The Pump, 1st and the 2nd Stokes signals wavelengths, GVD values and corresponding walk-off times between them.

Pump signal	*1st Stokes signal*	*2nd Stokes signal*	*Walk – off Pump & 1st Stokes*	*Walk – off 1st & 2nd Stokes*
$1060nm$ $0.23(ps^2/km)$	$1109nm$ $-0.06(ps^2/km)$	$1163nm$ $-0.28(ps^2/km)$	$0.49ps$	$1.08ps$
$1080nm$ $0.09(ps^2/km)$	$1131nm$ $-0.14(ps^2/km)$	$1187nm$ $-0.41(ps^2/km)$	$0.51ps$	$2.44ps$
$1100nm$ $0(ps^2/km)$	$1153nm$ $-0.28(ps^2/km)$	$1211nm$ $-0.51(ps^2/km)$	$1.06ps$	$2.9ps$
$1120nm$ $-0.1(ps^2/km)$	$1175nm$ $-0.37(ps^2/km)$	$1235nm$ $-0.61(ps^2/km)$	$1.92ps$	$3.9ps$
$1140nm$ $-0.21(ps^2/km)$	$1197nm$ $-0.46(ps^2/km)$	$1260nm$ $-0.67(ps^2/km)$	$2.85ps$	$4.41ps$

In the following cases, especially the effects of the pump power, GVD parameter (β_2) and fiber loss, on the generation of 1st and 2nd order Stokes pulses is summarized.

Case 1: ($\lambda_p = 1100nm \; and \; \alpha = 0.4dB/km$). At constant dispersion and fiber loss, pump power is varied from 3.56W to 5.7W. Particular results obtained for power levels at 3.56W, 3.64W and 4.94W are presented below for discussion.

Power level of 3.56W demonstrates near threshold behavior. When the pump power is close to threshold, the first order Stokes signal starts to build up inside the cavity and reaches to steady state without breaking up. If the power of the 1st order Stokes signal at steady state exceeds the threshold, it amplifies the 2nd order Stokes signal. Thus, the first

order Stokes signal starts to deplete and reaches its final steady state power at which the gain and the loss acting on the second order Stokes signal become equal. Since the saturation effect becomes negligible for low powers, any increase in the pump power within an allowable range, does not cause a significant change in the final steady state power of the 1st order Stokes signal. The additional energy from the pump is transferred to amplify the 2nd order Stokes signal more. To generate stable Stokes pulses at the output, it is required for the pulses to converge almost to a fundamental soliton where the peak power and the pulse width are related as $N^2 = P_0 \gamma \frac{T_0^2}{|\beta_2|} = 1$.

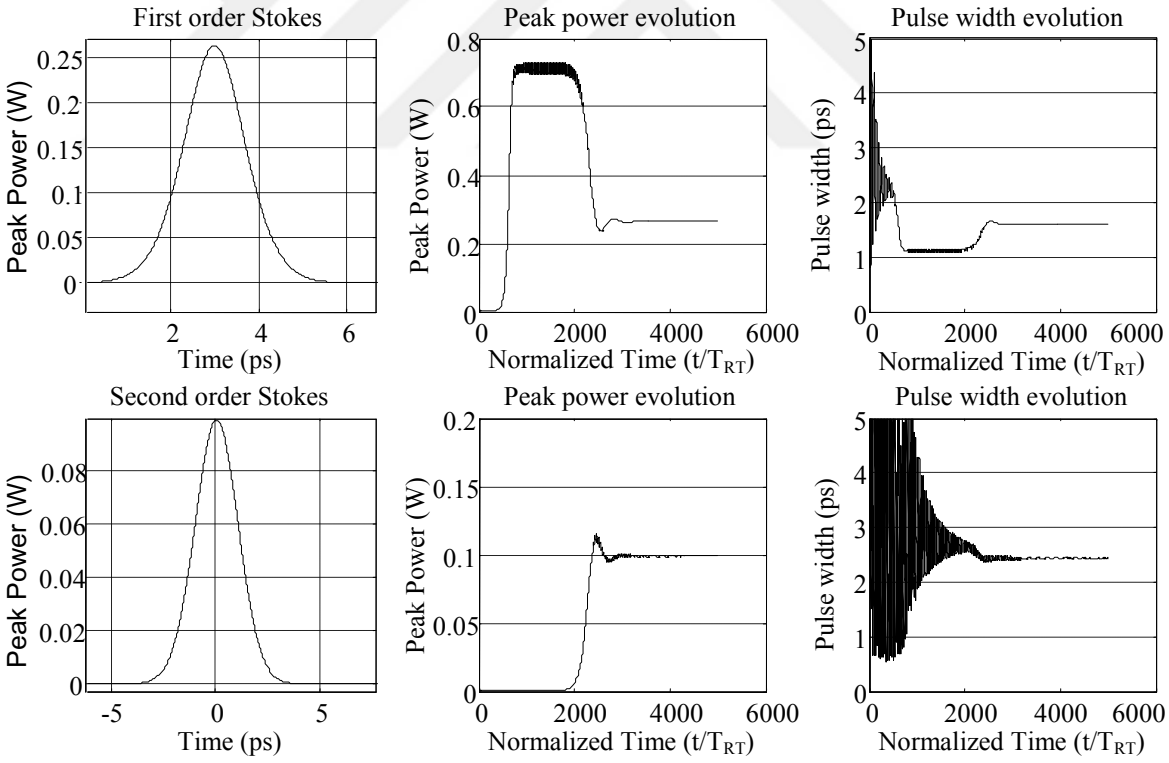

Fig. 3.5 $\lambda_p = 1100nm \; and \; \alpha = 0.4 dB/km$ at $P_p = 3.56W$.

When the pump power is increased to 3.64W, 1st order Stokes signal cannot preserve its stability and breaks up due to nonlinear effects. Since the Raman effect is an

instantaneous process, instability of the 1st order Stokes signal also distorts the evolution of the 2nd order Stokes signal. However, since the final expected powers of the Stokes signals are in stable region, they reach to steady state and converge to a soliton.

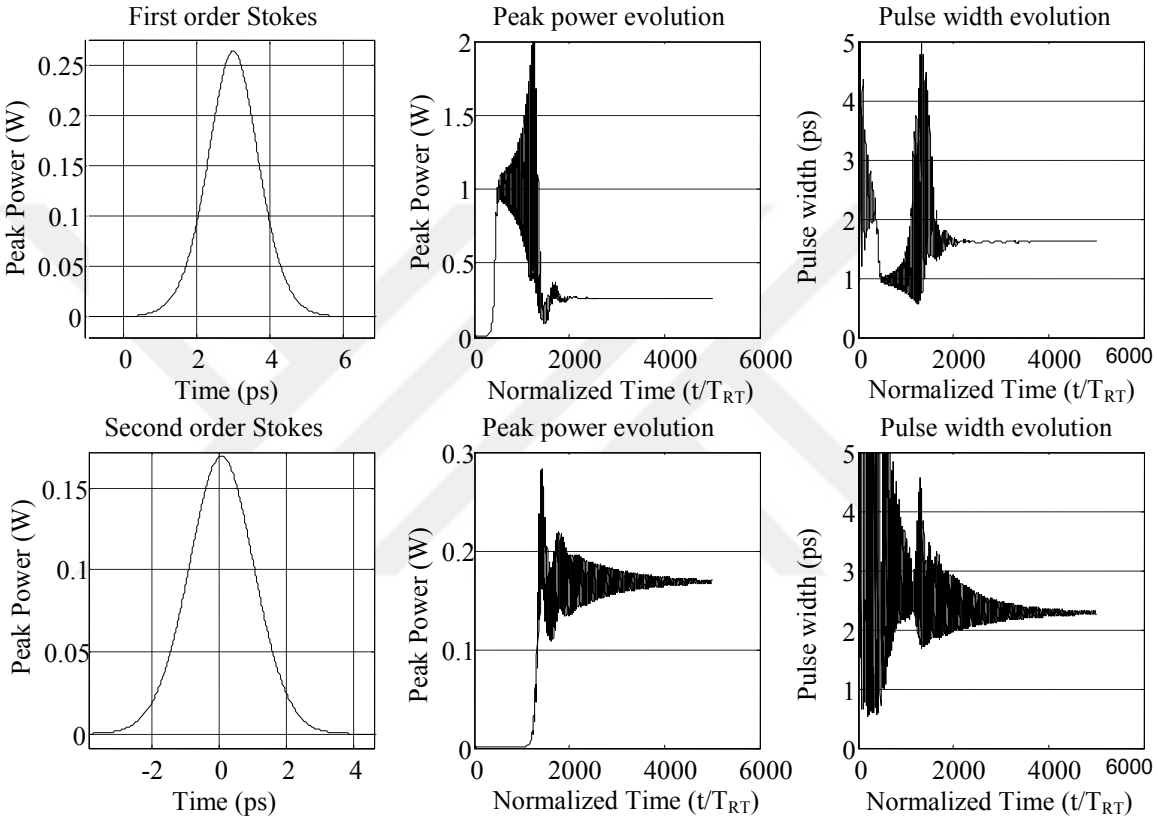

Fig. 3.6 $\lambda_p = 1100nm \; and \; \alpha = 0.4 dB/km$ at $P_p = 3.64W$.

As the pump power is increased beyond 4.5 Watts the power of the second order Stokes signal increases beyond the stable region, such as the results obtained for the power level of 4.94W. As a result of excessive power, 2nd order Stokes signal starts to break up. The insatiability in 2nd order also distorts the stability of 1st order Stokes signal.

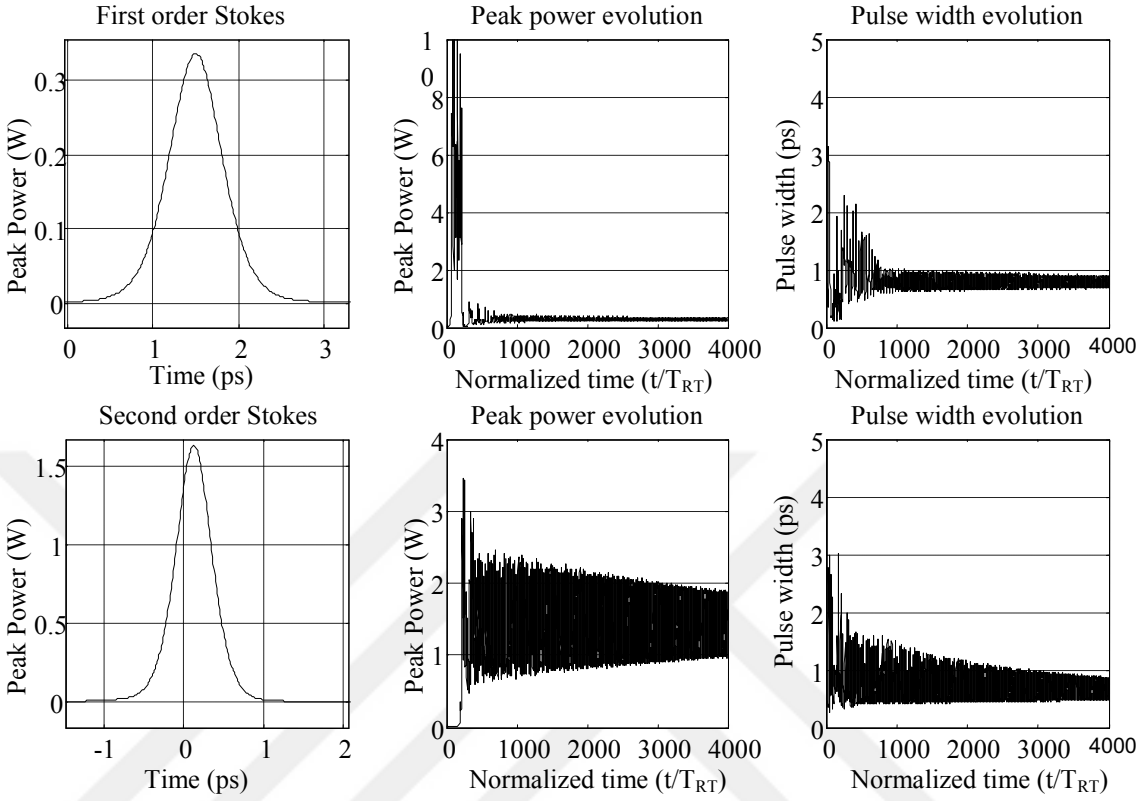

Fig. 3.7 $\lambda_p = 1100nm \; and \; \alpha = 0.4 dB/km$ at $P_p = 4.94W$.

Case 2: ($\lambda_p = 1100nm \; and \; P_p = 3.68W$) At constant dispersion and pump power, the simulation is repeated for such three different fiber loss conditions as $0.4 dB/km, 0.6 dB/km \; and \; 0.8 dB/km$..

The fiber loss due to different core compositions and design parameters affects propagation of the entire pump and the Stokes pulses. There are basically two different scenarios where the fiber loss affects the pulse evolution. In case of low pump power, the increase in the fiber loss prevents the generation of the Stokes signals since the gain cannot compensate the loss. On the other hand, if the pump power is high compared to threshold, the increase in the fiber loss raises the final steady state power of the 1st order

Stokes signal up and thus decreases the power of the 2nd order Stokes signal. As long as the final peak powers of the Stokes signals are in an allowable region where the nonlinear effects can be tolerated, Stokes pulses reach to steady state and converge to fundamental soliton. In particular, for 0.4dB/km fiber loss, since the attenuation is minimum (compared with the 0.6dB/km and 0.8dB/km fiber loss), the nonlinear effects are more pronounced and thus, it takes long time especially for second order Stokes signal to converge to its final power level.

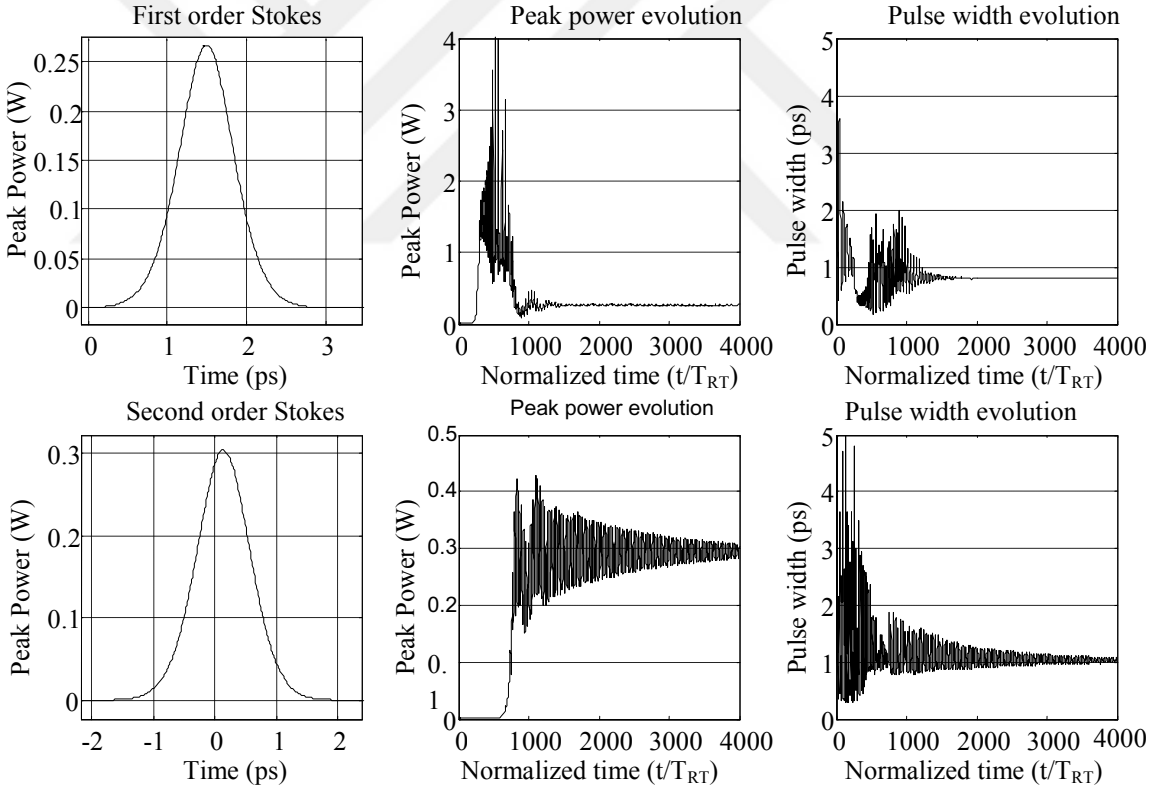

Fig. 3.8 $\lambda_p = 1100nm \; and \; P_p = 3.68W$ for $\alpha = 0.4dB/km.$

As the fiber loss is increased to 0.6dB/km, because of such two reasons as in a more lossy medium at the same pump power less nonlinear effects are pronounced and

the final expected pulses are in stable region, Stokes pulses immediately converge to their steady state power levels.

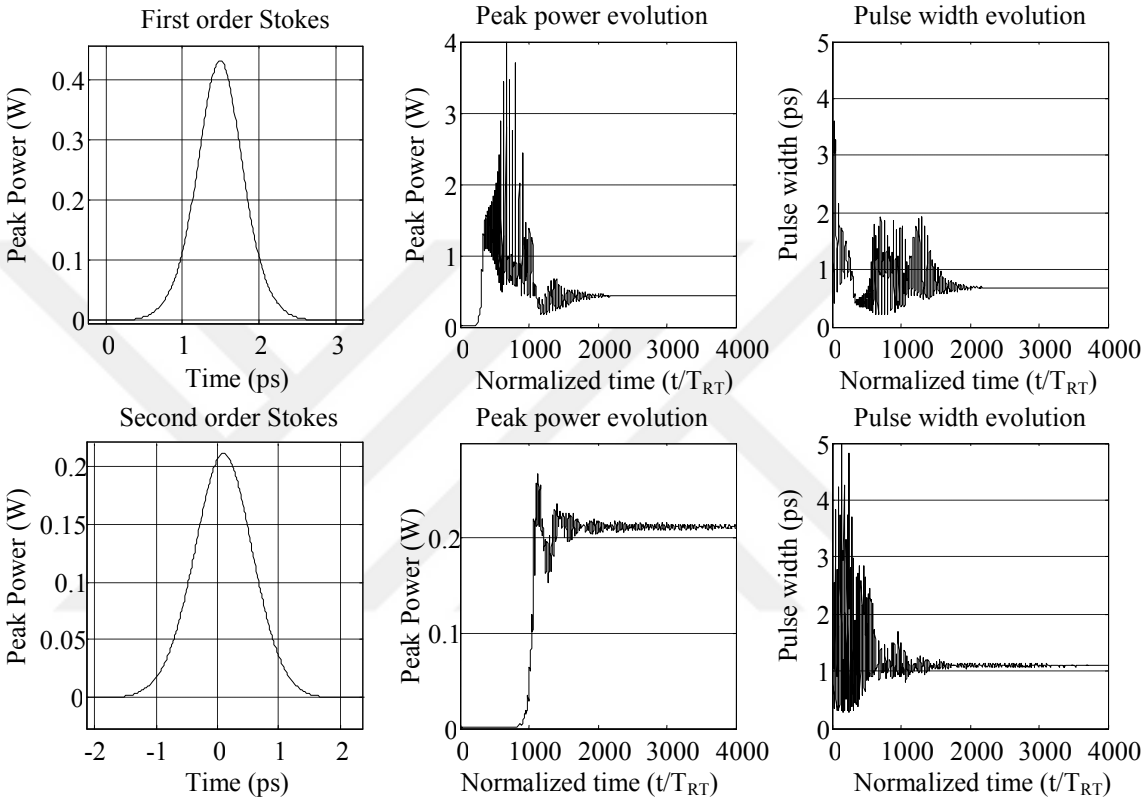

Fig. 3.9 $\lambda_p = 1100nm \; and \; P_p = 3.68W$ for $\alpha = 0.6dB/km.$

The simulation results performed for 0.8dB/km fiber loss, on the other hand, illustrates that the loss is quite high for the 2nd order Stokes signal to grow up more and deplete the power of the 1st order Stokes signal to stable levels. Although less nonlinear effect are pronounced due to high loss, in order to generate the 2nd order Stokes pulses more power is the required. Since, the 1st order Stokes signal cannot maintain its stability at high powers, both 1st and 2nd Stokes pulses start to break up.

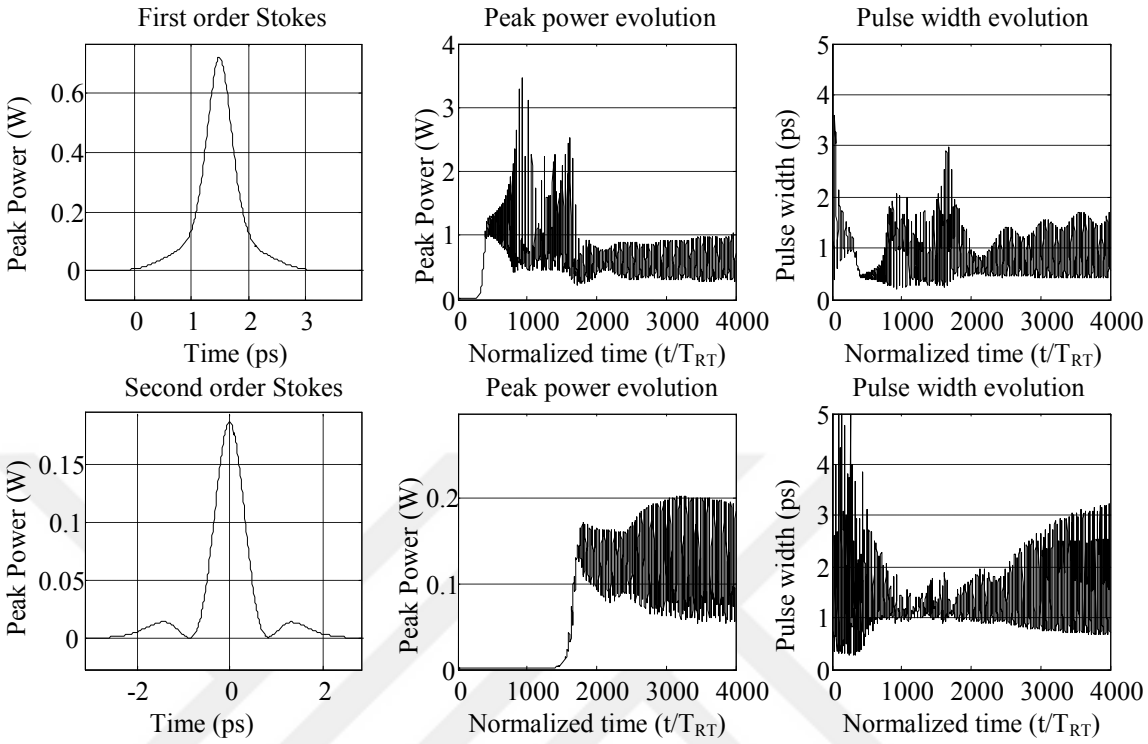

Fig. 3.10 $\lambda_p = 1100nm \; and \; P_p = 3.68W$ for $\alpha = 0.8dB/km.$

Case 3: ($P_p = 3.8W \; and \; \alpha = 0.4\,dB/km$) At constant pump power and the fiber loss, the GVD parameter (β_2) of the pump signal is varied from 0.23ps^2/km to -0.21 ps^2/km. The results performed at 0.23ps^2/km, 0ps^2/km and -0.21ps^2/km are presented in the following figures as an illustration.

By changing the zero dispersion wavelength of the fiber, the GVD parameters for each pump, 1st and the 2nd order Stokes pulse combination changes. Any change in the dispersion, as a result, alters the walk off between the pulses. Operating at higher GVD values causes an increase in the walk-off and leads the Stokes pulses to experience less gain in each round trip. This as a result, increases both the threshold to generate the 2nd order Stokes signal, i.e. 1st order Stokes signal with more power is needed, and the time

required for the pulses to reach the steady state. At $\beta_2^{pump} = 0.23 ps^2/km$, the 1st and the 2nd order Stokes signals with the smallest walk-off (1.08ps) between them instantly converge to stable soliton pulses with 0.17W and 0.35W peak powers, respectively.

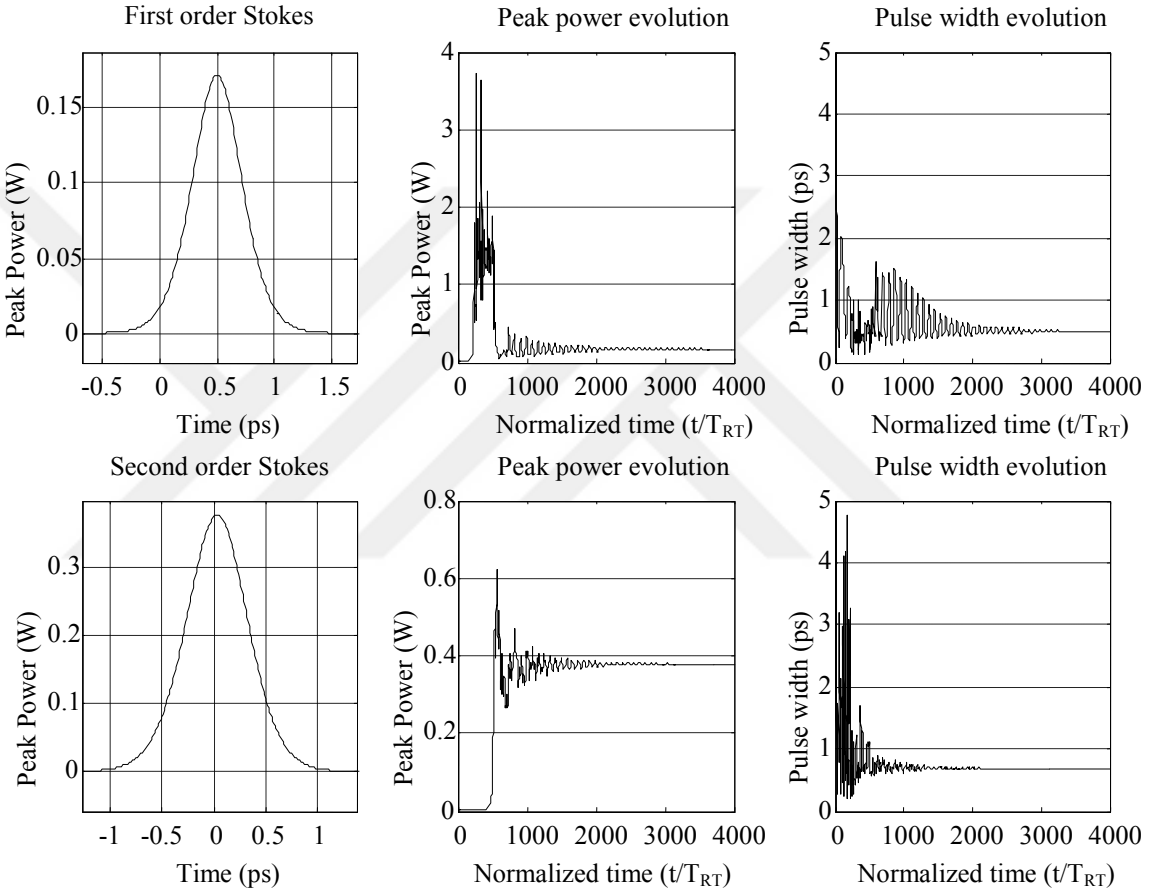

Fig. 3.11 $P_p = 3.8W \ and \ \alpha = 0.4 dB/km$ at $\beta_2 = 0.23 ps^2/km.$.

The walk-off between the Stokes pulses increases to 2.41ps at $\beta_2^{pump} = 0 ps^2/km$, and 4.41ps at $\beta_2^{pump} = -0.21 ps^2/km$. As seen in the following figures, increase in the walk-off leads the peak power of the 1st order Stokes signal to increase and the one for the second order Stokes signal to decrease. In addition, walk-off affects the convergence

rate such that the oscillations due to excessive nonlinear effects last for longer time. On the other hand, since the GVD parameter increases, the Stokes pulses become more robust to the nonlinear effects and the upper limit of the stable region may rise but with the slower convergence rate.

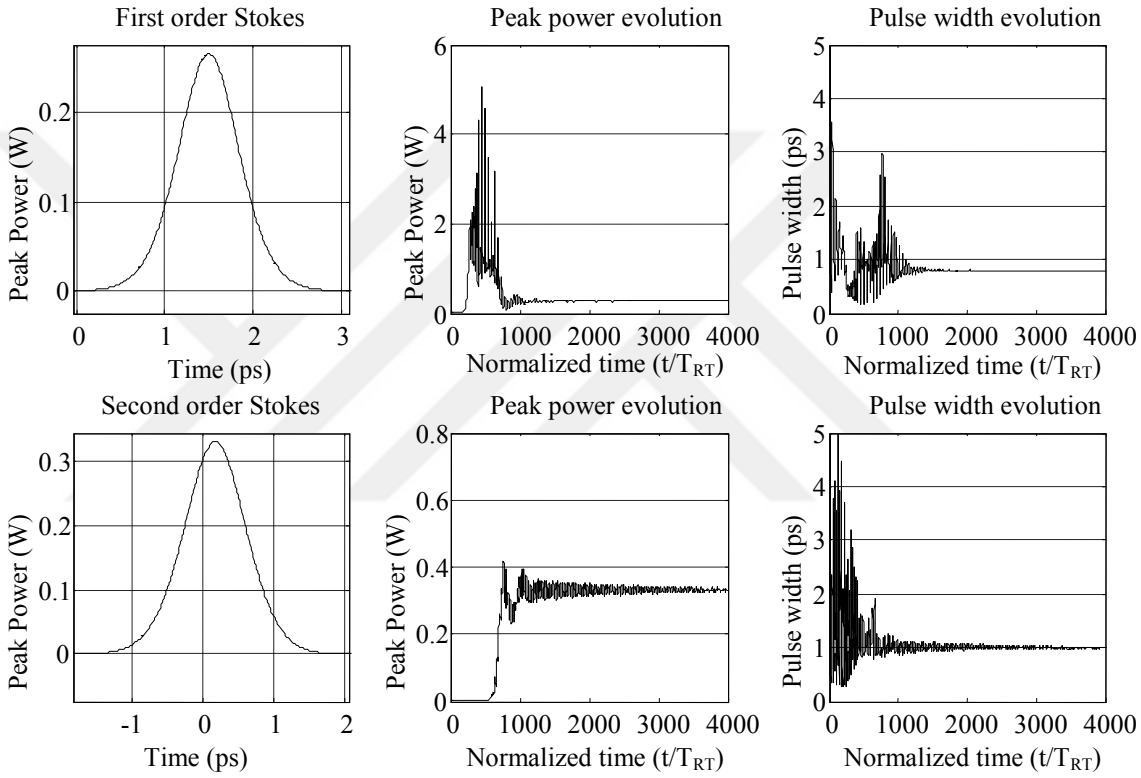

Fig. 3.12 $P_p = 3.8W \; and \; \alpha = 0.4\,dB/km \text{ at } \beta_2 = 0\,ps^2/km.$.

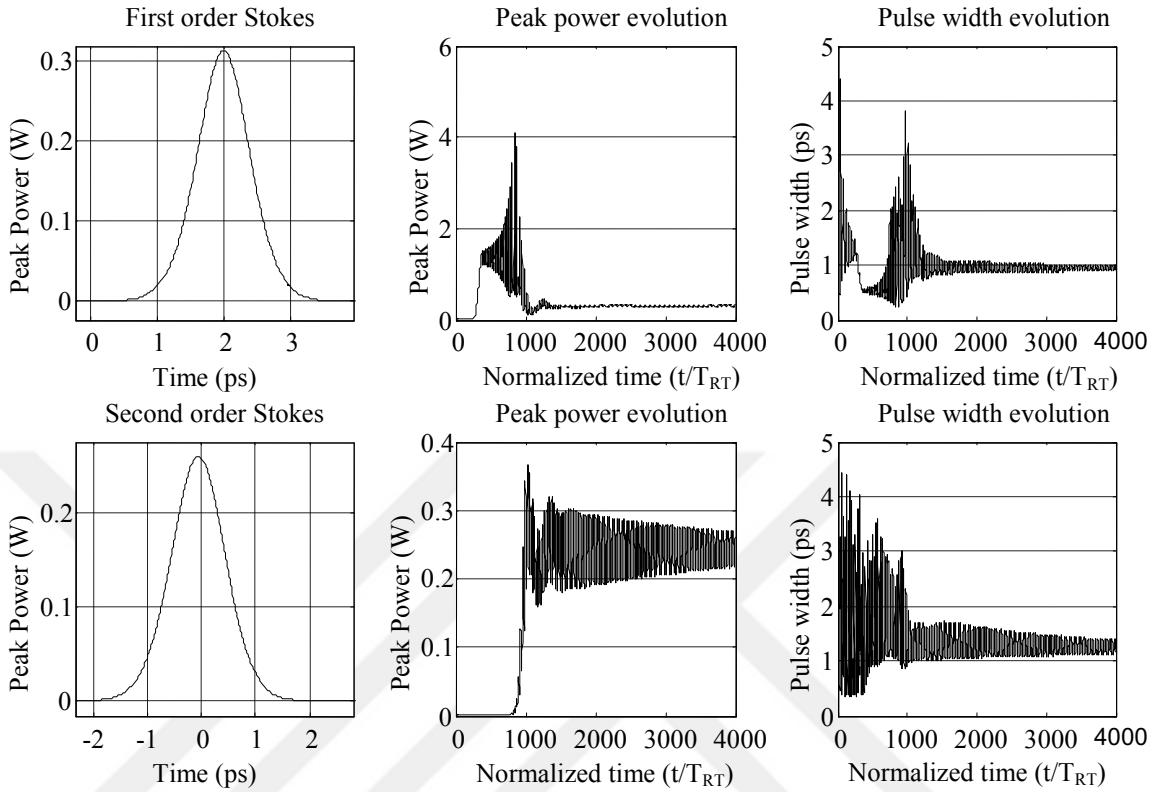

Fig. 3.13 $P_p = 3.8W \ and \ \alpha = 0.4\,dB/km$ at $\beta_2 = -0.21 ps^2/km.$).

3.4 The Stability Analyses

To assess the stability regime of the generated Stokes signals where they converge to a hyperbolic secant square soliton pulse, SSFM simulation was repeated for combinations of 5 different pump wavelengths and 8 pump powers. The output Stokes signals obtained from each simulation was analyzed and categorized with respect to their peak powers and pulse widths and results are represented in the following contour plots.

Figure 3.14 shows the peak powers and the pulse widths of the output Stokes pulses at specific GVD value (for the pump signal) and the pump power for the fiber with 0.4dB/km loss.

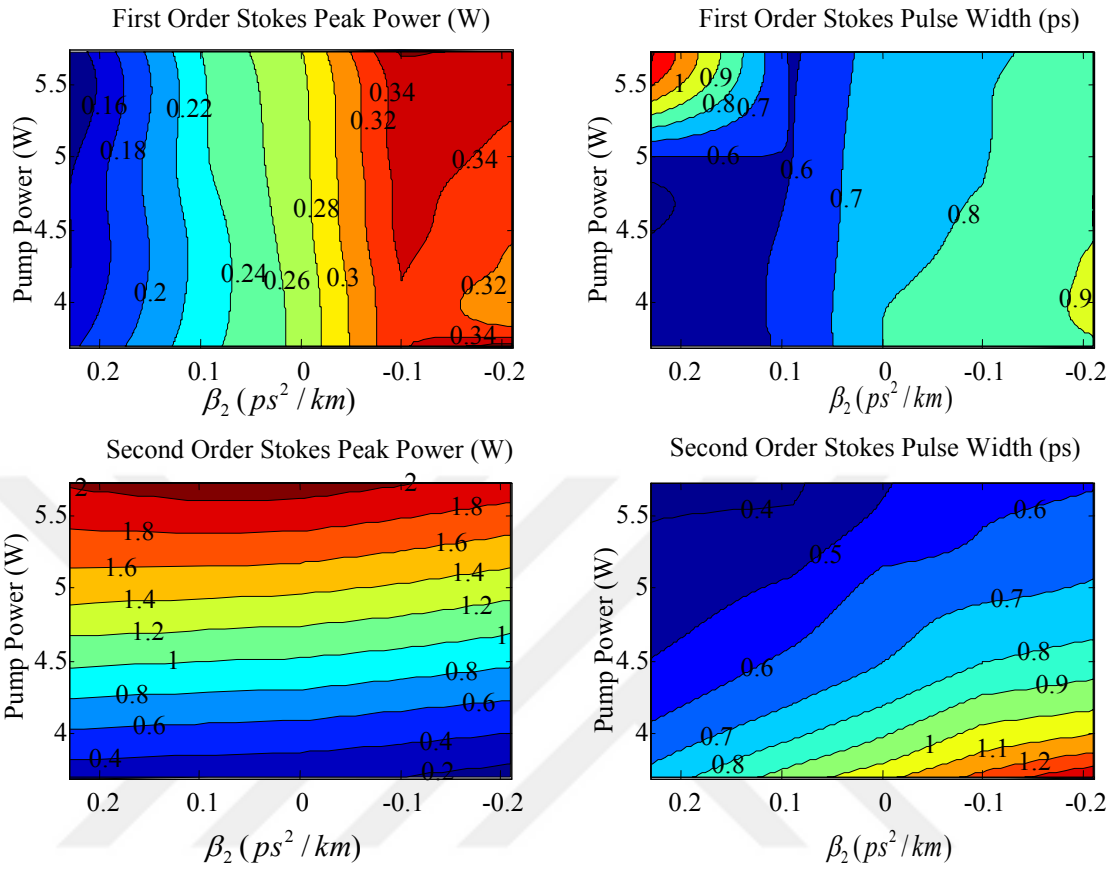

Fig. 3.14 Contour plots of 1st and 2nd order Stokes signals due to peak power and pulse width for the fiber loss 0.4dB/km (β_2 values due to Figure 3.4 belong to the pump signal).

As seen in the contour plots for 0.4dB/km fiber loss, the output Stokes pulses show a regular pattern. Since 1st order Stokes pulses converge to the peak power which is almost determined by the loss acting on the 2nd order Stokes signal at steady state, increase in the pump power has no significant effect on the peak powers and the pulse widths of the 1st order Stokes pulses at specific GVD. However, increase in the pump power provides an additional gain for the 2nd order Stokes pulses. Thus, while the peak powers of the 2nd order Stokes pulses increase, the pulse widths reduce to satisfy the fundamental soliton condition as $N^2 = \frac{T_0^2}{|\beta_2|} P_0 \gamma = 1$. In addition, since the walk-off is

more pronounced at high GVD values (such as β_2 = -0.41 to -0.68ps^2/km for the Stokes signals) in anomalous dispersion regime (at longer pump wavelengths), 2nd order Stokes pulses experience less gain and cannot deplete the 1st order Stokes pulses sufficiently. This, as a result, causes an increase in the peak powers of the 1st order Stokes pulses and a reduction in the peak powers of the 2nd order Stokes pulses. Pulse widths of the Stokes pulses at steady state, however, are determined by the fundamental soliton condition. As shown in the Figure 3.14, Stokes pulses generated at longer wavelengths (with high β_2 values) and at low pump powers converge to a soliton with larger pulse widths.

In the following contour plots, the effect of the fiber loss on the evolution of the Stokes pulses is illustrated for such two different fiber loss as 0.6dB/km and 0.8dB/km.

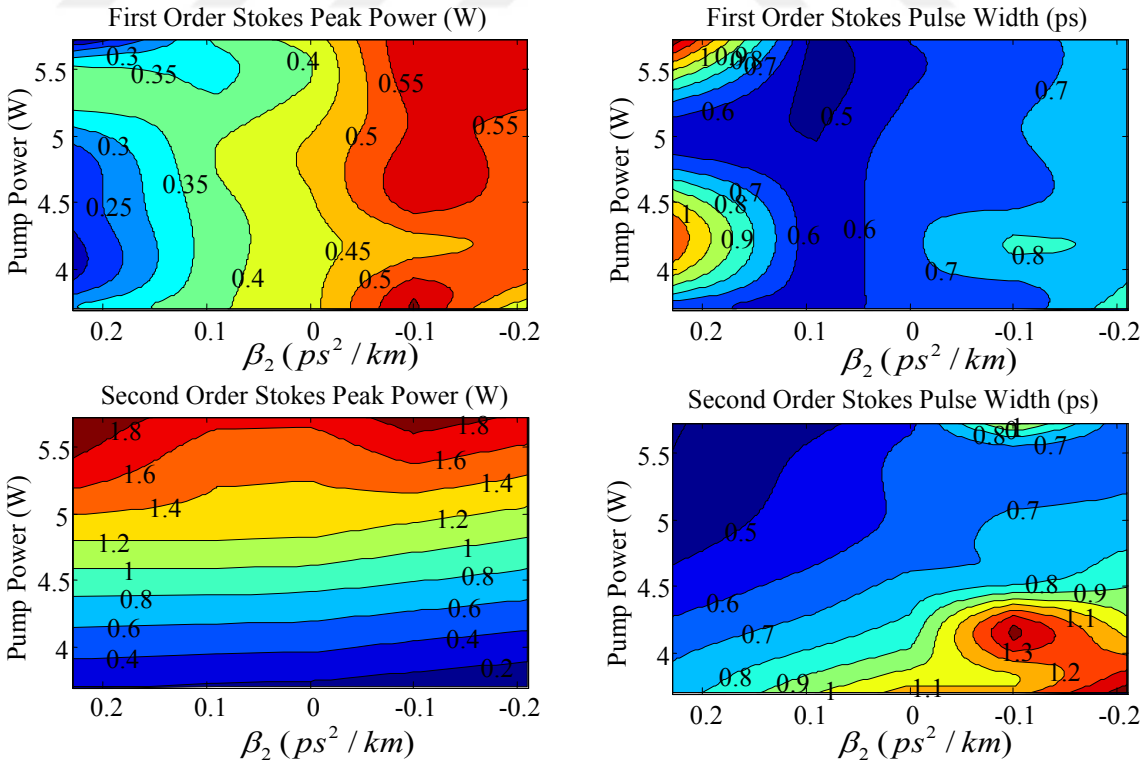

Fig. 3.15 Contour plots of 1st and 2nd order Stokes signals due to peak power and pulse width for the fiber loss 0.6dB/km. (β_2 values due to Figure 3.4 belong to the pump signal).

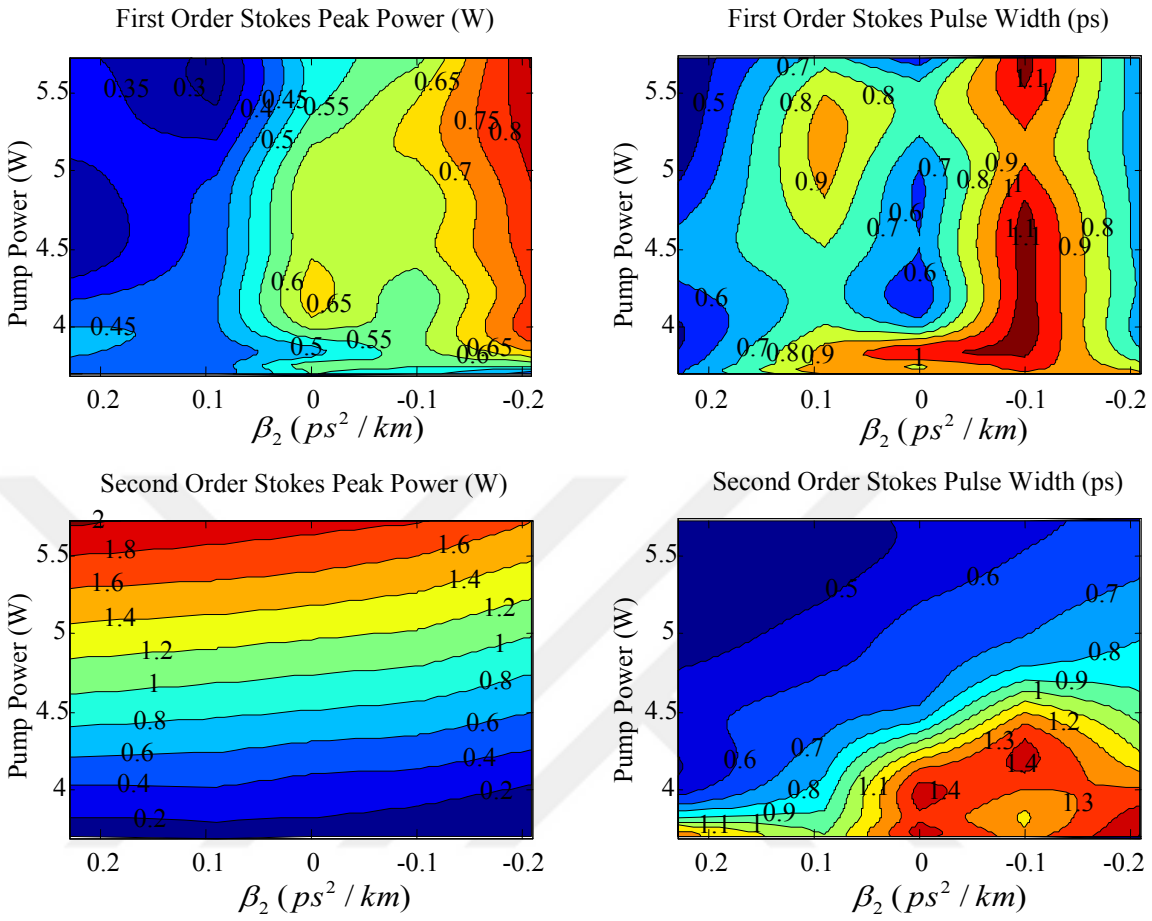

Fig. 3.16 Contour plots of 1st and 2nd order Stokes signals due to peak power and pulse width for the fiber loss 0.8dB/km (β_2 values due to Figure 3.4 belong to the pump signal).

Fiber loss is the common term that defines the cavity losses acting on the both Stokes pulses. Any increase in the fiber loss, causes more attenuation in the entire pump and the Stokes pulses which as a result lead the gain experienced by the Stokes pulses to decrease. In addition, since the threshold to generate the Stokes pulses is directly proportional with the fiber loss, more power is required for the Stokes pulses to build up and converge to steady state. Thus, at low pump powers especially the 2nd order Stokes pulses cannot be generated due to insufficient power levels. When we analyze the contour plots for the 2nd order Stokes pulses carefully, it can be seen that, the dark region at the

bottom which corresponds to unsaturated (below or close to threshold) output Stokes pulses at low pump powers, increases with the fiber loss. Also, at the same pumping conditions (same pump power and GVD) with enough power to generate the Stokes pulses, increase in the fiber loss leads the 1st order Stokes pulses to converge to high powers because the second order Stokes do not have enough power to deplete the first order Stokes. As a result of an increase in the steady state powers of the 1st order Stokes pulses, the nonlinear effects become more pronounced and unless being in a stable region where the nonlinear effects can be totally compensated, pulses start to break up. The irregularity in the contour plots especially for the 1st order Stokes pulses indicates the break up regions and increases with the fiber loss.

CHAPTER 4

CONCLUSIONS AND SUMMARY

The nonlinear interactions that lead to generation of a Raman Soliton laser such as soliton formation and Raman scattering are discussed and a theoretical model which aims to assign the design criteria for especially 1^{st} and the 2^{nd} order Raman soliton lasers was developed. Split Step Fourier Method is used as a numerical method to simulate the governing propagation equations for the pulses. Stability analyses for 1^{st} and the 2^{nd} order Raman soliton lasers are conducted for the parameters from existing fibers. To conclude, it is showed that if the proper dispersion and pumping conditions are met, high power stable soliton pulses at 1^{st} and the 2^{nd} order Stokes wavelengths with sub-picosecond pulse widths varying from 300fs to 1ps can be generated.

Due to its potential for delivering wavelength tunable, high power, stable output pulses with $1000cm^{-1}$ spectral separation, Raman soliton lasers will find applications in many areas such as spectroscopy, sensing, communication and microscopy.

REFERENCES

[1] C.J.S. Matos, S.V. Popov, and J.R. Taylor, "Short-pulse, all-fiber, Raman laser with dispersion compensation in a holey fiber", Opt. Lett. Vol. 28, No. 20 (2003).

[2] G H. Renner, S. Cierullies, M. Krause, "Scaling rules for Raman fiber lasers", Optical Fiber Communication Conference (OFC), Atlanta, USA (Paper MF25), (2003).

[3] M. Krause, H. Renner, "Theory and design of double-cavity Raman Fiber Laser", J. Lightwave Technology, Vol. 23, No. 8 (2005).

[4] S. Cierullies, H. Renner, E. Brinkmeyer, "Numerical optimization of multi-wavelength and cascaded Raman fiber lasers", Opt. Commun. 217(1-6), pp. 233-238 (2003).

[5] G.P. Agrawal, Nonlinear Fiber Optics 4th edition. (Academic Press 2009)

[6] G.P. Agrawal, Fiber Optic Communication Systems 3rd edition. (Academic Press 2002)

[7] M.N. Islam, L.F. Mollenauer and R.H. Stolen, "Cross-phase modulation in optical fibers", Opt. Lett., vol. 12, no. 8, 1987.

[8] C.V. Raman, Indian Journal Phys. 2,387 (1928).

[9] E.J. Woodbury and W.K. Ng, "Ruby laser operation in near IR" Proc IRE 50, 2347 (1962).

[10] R.W. Boyd, Nonlinear Optics, 2nd edition. (Academic Press 2003)

[11] R.H. Stolen, in Raman Amplifiers for Telecommunications, Part 1, M.N. Islam, Chap. 2 (Springer 2004).

[12] R. Shuker and R.W. Gammon, "Raman scattering selection rule breaking and density of states in amorphous materials", Phys. Rev. Lett. 25, 22 (1970).

[13] D. Hollenbeck, C.D. Cantrell, "Multi-vibrational-mode model for fiber-optic Raman gain spectrum and response function", J. Soc. Am. B/Vol. 19, No. 12 (2002).

[14] H. Hasegava and Y. Kodama, Solitons in Optical Communication, Oxford University Press, 1995.

[15] H. Hasegawa and Y. Kodama, Proc. IEEE 69, 1145 (1981), Opt. Lett. 7, 285 (1982).

[16] M. Nakazawa, K. Suzuki, Y. Kimura, "3.2-5 Gb/s, 100km error free soliton transmissions with Erbium amplifiers and repeaters" IEEE Photon. Techno. Lett. 2, 216 (1990).

[17] T.E. Murphy, "Soliton Pulse Propagation in Optical Fiber" (2001).

http://www.photonics.umd.edu/pubs/misc-presentations/MP-1/solitons.pdf

[18] H.A. Haus, M. Nakazawa, "Theory of fiber Raman soliton laser", J. Opt. Soc. Am. B/Vol. 4, No. 5, (1987).

[19] W.H. Reeves, J.C. Knight, and P.St.J. Russell, "Demonstration of ultra-flattened dispersion in photonic crystal fibers", Vol. 10, No. 14 / Opt. Express (2002).

[20] H. Rong, S. Xu, O. Cohen, O. Raday, M. Lee, V. S and M. Paniccia, “A Cascaded Silicon Raman Laser”, Nature Photonics 2, 170-174 (2008).

[21] B. Washburn, “Numerical Solutions to Nonlinear Schrödinger Equation”.

http://www.phys.ksu.edu/personal/washburn/pdf/washburn_thesis_chapter4.pdf